

**An Exploration of Thermomechanical Softwood Pulp for N95 Respiratory
Mask Production**

By: Kaleigh Elizabeth Rita McLeod

A Thesis Submitted to

Saint Mary's University, Halifax, Nova Scotia

In Partial Fulfilment of the Requirements for the Degree of
Bachelor of Science with Honours in Chemistry

April 2021, Halifax, Nova Scotia

Copyright Kaleigh Elizabeth Rita McLeod, 2021

Supervisor: Dr. Christa Brosseau

Co-Supervisor: Dr. Robert Singer

Department Chair: Dr. Jason Masuda

Date: April 26, 2021

Certification

An Exploration of Thermomechanical Softwood Pulp for N95 Respiratory Mask Production

By: Kaleigh Elizabeth Rita McLeod

Copyright Kaleigh Elizabeth Rita McLeod, 2021

I hereby certify that this thesis was completed by Kaleigh Elizabeth Rita McLeod in partial fulfillment of the requirements of the Degree of Bachelor of Science with Honours in Chemistry at Saint Mary's University and I certify that this is truly the original work carried out by Kaleigh Elizabeth Rita McLeod.

Thesis Supervisor

Dr. Christa L. Brosseau

Thesis Co-Supervisor

Dr. Robert Singer

Chairperson of the Chemistry Department

Dr. Jason D. Masuda

Date: April 26, 2021

Abstract

An Exploration of Thermomechanical Softwood Pulp for N95 Respiratory Mask Production

By: Kaleigh Elizabeth Rita McLeod

The COVID-19 pandemic has highlighted supply chain issues for personal protective equipment (PPE) in Canada. In addition, many PPE products are produced from non-renewable feedstocks. Wood pulp is an abundant and renewable natural resource. Currently, wood pulp from one Canadian paper mill in particular is used in combination with synthetic polymers, such as polypropylene, to produce non-woven textiles. Most of the world's population has become familiar with non-woven textiles over the course of 2020 since they are used to produce the 3-ply disposable masks that many people are currently required to wear. Not only are the synthetic polymers produced with the use of solvents that are detrimental to the environment, but these single use masks are piling up in landfills.

The goal of this project was to work in partnership with Port Hawkesbury Paper to produce PPE entirely out of Nova Scotian thermomechanical wood pulp (TMP). This pulp is produced in a low effluent mechanical process that uses less harsh chemicals than the production of synthetic polymers. Above all, wood pulp based PPE would be biodegradable, therefore this would have an enormously positive impact on the population's waste output.

Overall, this thesis work reviews characteristics of existing PPE and the impact of lignin content on filtration efficiency of pulp fibers. Lastly, chemical modification with deep eutectic solvents is explored to investigate their potential to improve filtration capabilities.

Acknowledgements

I would like to thank my research supervisors Dr. Christa Brosseau and Dr. Robert Singer for their support and guidance. I especially want to extend my thanks to Dr. Brosseau for supervising me over the past three years. Dr. Brosseau demonstrates all of qualities I could ever of dreamed of having in a research supervisor. I would also like to thank the current and past Brosseau lab group members: Dalal Alhatab, Najwan Albarghouthi, Kathleen Allen, Stephanie Amrieh, Shruti Bindesri, Makatendeka Biton, James Crighton, Melanie Davidson, Raynier De Bellotte, Maddy Eisnor, Carolyn Farling, Tanner George, Megan Himmelman, Nusrat Jahan, Mojan Jahanbiglary, Amir Joorab Doozha, Sam Julien, Marissa MacInnis, Pema Sherpa, Gaius St. Marie, Mary Stackaruk, and especially Taylor Lynk for being my mentor.

In response to the COVID-19 pandemic I am grateful for the opportunity I have had to work on the “Pulp Project”. This team specifically was comprised of Carolyn, Megan, Nusrat, Sam and myself. Megan came up with this idea, Carolyn and Nusrat worked mainly on Kappa number determination, Sam and Nusrat worked on deep eutectic solvent treatments, and I worked on PPE characterization and filtration studies.

I would also like to extend my appreciation to our chemistry technicians Elizabeth McLeod, Alyssa Doué, and Patricia Granados. I am so fortunate to have had the opportunity to be a part of such a supportive and close knit chemistry department. Thank you to the faculty of chemistry for teaching me. Also, I appreciate Dr. Xiang Yang for his assistance in operating the SEM over the past three years.

Lastly, I want to thank my friends, old and new, and family for their encouragement and love. I want to thank my parents for their support but especially my Mother, for encouraging me to come to St. Mary’s, to study chemistry, and always supporting me in all of my endeavours.

Table of Contents	Page #
Abstract.....	iii
Acknowledgments.....	iv
List of Figures	vi
List of Tables.....	vii
List of Abbreviations	viii
CHAPTER 1: INTRODUCTION.....	1
1.1 RESEARCH GOAL.....	1
1.2 INTRODUCTION.....	1
1.3 LITERATURE REVIEW	2
1.3.1 Viruses	2
1.3.2 Masks.....	3
1.3.3 Wood Pulp and Papermaking.....	6
1.3.4 Cellulose Based Filtration.....	8
1.3.5 Lignin.....	9
1.3.6 Deep Eutectic Solvents	13
1.3.7 Kappa Number.....	15
1.3.8 Fluorescence Spectroscopy	15
1.3.9 Aerosol Testing.....	16
1.4 THEORY	19
1.4.1 Wood Pulping.....	19
1.4.2 Spectroscopic Methods for Lignin Detection	19
1.4.3 Deep Eutectic Solvents	20
1.4.4 Kappa Number.....	21
1.4.5 Fluorescence.....	22
1.4.6 Aerosol Testing.....	23
CHAPTER 2: EXPERIMENTAL.....	25
2.1 SHEET FORMING.....	25
2.2 KAPPA NUMBER	26
2.3 INFRARED SPECTROSCOPY.....	27
2.4 DEEP EUTECTIC SOLVENT	27
2.5 FLUORESCENCE TESTING.....	29
2.6 MANNEQUIN HEAD AEROSOL TEST.....	29
2.7 SCANNING ELECTION MICROSCOPY STUDIES	30
CHAPTER 3: RESULTS AND DISCUSSION	31
3.1 CHARACTERIZATION OF COMMERCIAL PERSONAL PROTECTIVE EQUIPMENT	31
3.2 CHARACTERIZATION OF PULP SAMPLES	37
3.3 DEEP EUTECTIC TREATMENT OF PULP SAMPLES	41
3.4 SHEET THICKNESS	44

3.5 FLUORESCENCE SPECTROSCOPY: FILTRATION EFFICIENCY	45
3.6 AEROSOL TESTS	51
CHAPTER 4: CONCLUSIONS	53
CHAPTER 5: FUTURE WORK.....	55
CHAPTER 6: REFERENCES.....	56
CHAPTER 7: APPENDIX.....	60
7.1 SEM IMAGES OF FILTER PAPER FOLLOWING FILTRATION.....	60
7.2 REPRODUCED FIGURES LETTERS OF PERMISSION	61

List of Figures

Page #

Figure 1-1: The cumulative Canadian COVID-19 case data showing (A) the number of daily new confirmed cases per million people and (B) the number of cumulative confirmed cases. Image reproduced with permission from Rosser et al. 2021. ⁵	2
Figure 1-2: Diagram of the basic components of an enveloped virus.	3
Figure 1-3: Comparison of filtration efficiencies of four mask types including N95, Dust/Fume/Mist (DFM), Dust/Mist (DM) and surgical measured at a flow rate of (A) 85 L/min and (B) 32 L/min. Image reproduced with permission from Qian et al. ⁸	5
Figure 1-4: The chemical structure of cellulose.	6
Figure 1-5: A scheme depicting the hierarchical structure of a wood fiber. Image reproduced with permission from Zhu et al. ¹⁷	7
Figure 1-6: The main bond linkages present in softwood lignin. Image adapted from Laurichesse et al. ²³ Bolded bonds are included to clearly indicate the lignin linkages.	10
Figure 1-7: The three monolignol precursors and their structures within lignin polymers. Image reproduced with permission from Laurichesse et al. ²³	11
Figure 1-8: The proposed choline chloride: urea DES interaction with an eutectic point at a 1:2 ratio. Image adapted from Ashworth et al. ³²	13
Figure 1-9: Choline chloride: oxalic acid DES interaction. Image adapted from Wang et al. ³³ .	14
Figure 1-10: The fluorospectrophotometric profiles measured for of the blank pure solvent, the start solution containing the fluorophore, and the filtrate following filtration with the nanocellulose. The size of fluorescent beads used for each experiment varied (a) 500 nm, (b) 100 nm, and (c) 30 nm. Each results is the average of three measurements. The photograph inlet on each plot is the Cladophora membranes following the filtration. Image reproduced with permission from Metreveli et al. ¹⁸	16
Figure 1-11: The (a) schematic of the instrumentation required for the rapid aerosol testing method and (b) the data output received from this experimental set-up. Image reproduced with permission from Schilling et al. ³⁶	17
Figure 1-12: Experimental set-up to test mask aerosol filtration. Where (a) is a mannequin head, (b) is a vacuum pump, (c) is tubing, (d) is a sealing mixing chamber, and (e) is a GRIMM Aerosol Spectrometer. Imaged reproduced from Faridi et al. ³⁷	18
Figure 1-13: Kraft cleavage of β -O-4 aryl ether linkages in lignin. Image adapted from Froass et al. ³⁸	19
Figure 1-14: The phase diagram showing the eutectic point for a specific composition of components A and B.....	21
Figure 1-15: The energy level diagram represents the changes in electronic state in (a) molecular absorption, (b) nonradiative relaxation, and (c) fluorescence. Image adapted from Skoog et al. ⁴³	23
Figure 2-1: Flow chart of the paper sheet forming process.	26
Figure 2-2: The mannequin head set up for aerosol testing.....	30
Figure 3-1: (a) The 3M brand N95 mask. The 3M mask is a NIOSH certified three layer N95 mask. (b) The SEM image of the middle filter layer of the 3M mask. SEM (voltage: 5.0 keV, Det: SE, Tescan MIRA3 LMU Field Emission SEM).....	31

Figure 3-2: The FTIR spectra of the three layers of the 3M N95 mask.	32
Figure 3-3: (a) The DEGiL brand N95 mask. The DEGiL mask is a NIOSH certified three layer N95 mask. (b) The SEM image of the middle filter layer of the DEGiL mask. SEM (voltage: 5.0 keV, Det: SE, Tescan MIRA3 LMU Field Emission SEM).....	33
Figure 3-4: The ATR-FTIR spectra of the three layers that compose the DEGiL N95 mask.	33
Figure 3-5: (a) The InterMask ^(TM) 3 Ply Disposable Face Mask. (b) The SEM image of the middle filter layer of the InterMask ^(TM) 3 Ply Disposable Face Mask. SEM (voltage: 5.0 keV, Det: SE, Tescan MIRA3 LMU Field Emission SEM).....	34
Figure 3-6: The ATR-FTIR spectra of the three layers that compose the InterMask ^(TM) 3 Ply Disposable Face Mask.	34
Figure 3-7: SEM characterization of the outer fabric layer of various personal protective equipment including (a) a disposable isolation gown, (b) the 3M N95 mask, (c) the DEGiL N95 mask, and the InterMask ^(TM) 3 Ply Disposable Face Mask. SEM (voltage: 5.0 keV, Det: SE, Tescan MIRA3 LMU Field Emission SEM).	35
Figure 3-8: Cellulose based mask support layer distributed by Ahlstrom Monksjo. Including (a) DRAPE Wetlaid and (b) DRAPE Sterilization Economy Plus.	36
Figure 3-9: FTIR of DRAPE Wetlaid Ahlstrom Monksjo Mask Support Layer fabric.....	36
Figure 3-10: The pulp samples as received from Port Hawkesbury Paper.....	38
Figure 3-11: SEM Images of unmodified pulp samples (A & B) R1B, (C & D) R2B, and (E & F) SPD. SEM (voltage: 5.0 keV, Det: SE, Tescan MIRA3 LMU Field Emission SEM).	39
Figure 3-12: Untreated MC6 hand sheet. SEM (voltage: 5.0 keV, Det: SE, Tescan MIRA3 LMU Field Emission SEM).	40
Figure 3-13: SEM-EDX analysis of an Untreated MC6 hand sheet. SEM (voltage: 5.0 keV, Det: SE, Tescan MIRA3 LMU Field Emission SEM).	40
Figure 3-14: L1LAT Pulp (A) Untreated, (B) DES14-A Treated, DES14-B Treated. SEM (voltage: 5.0 keV, Det: SE, Tescan MIRA3 LMU Field Emission SEM).	43
Figure 3-15: The excitation and emission scans stacked for a 1.56×10^{-4} % solids 0.1 μm fluorescent bead suspension. The excitation peak appeared at 540 nm and the emission peak appeared at 583 nm. Fluorescent scans were taken using a Agilent Cary Eclipse fluorescence spectrophotometer.	45
Figure 3-16: The more dilute calibration curve for the 0.1 μm fluorescent bead suspension in ASTM Type 1 water.....	46
Figure 3-17: The calibration curve for the 0.1 μm fluorescent bead suspension in ASTM Type 1 water.	46
Figure 3-18: The calibration curve for the 0.3 μm fluorescent bead suspension in ASTM Type 1 water.	49
Figure 3-19: The final paper products produced by Port Hawkesbury both (A) Uncalendared and (B) Super-Calendared. SEM (voltage: 5.0 keV, Det: SE, Tescan MIRA3 LMU Field Emission SEM).....	50
Figure 7-1: The SEM images of filtration paper following filtration of 100 nm fluorescent beads. (A) and (B) are R1B 0.25mm, (C) and (D) are R2B 0.25 mm, (E) and (F) are K10s 1.26 mm. SEM (voltage: 5.0 keV, Det: SE, Tescan MIRA3 LMU Field Emission SEM).	60

Figure 7-2: The SEM images of filtration paper following filtration of 300 nm fluorescent beads. (A) and (B) are L2LAT, (C) and (D) are R2B, (E) and (F) are Screen Accepts. SEM (voltage: 5.0 keV, Det: SE, Tescan MIRA3 LMU Field Emission SEM..... 61

List of Tables	Page #
Table 1-1: Comparison of Kraft Pulp to TMP. ²⁰	9
Table 1-2: Common DES molar ratios and melting points. Table adapted from Tang and Row. ³⁴	14
Table 2-1: DES Reaction Conditions	28
Table 3-1: Spectral band assignments of ATR-FTIR of DRAPE Wetlaid Ahlstrom Monksjo mask support layer fabric.	37
Table 3-2: Kappa number results for untreated and DES treated pulps.....	41
Table 3-3: DES Reaction Yields.....	42
Table 3-4: The thickness of various combinations of N95 mask layers. Compressed here refers to if pressure is place on the material during thickness measurements.	44
Table 3-5: The thickness of each of the tested paper sheets.	44
Table 3-6: The 10 blank reads taken with $\lambda_{ex} = 540$ nm and $\lambda_{em} = 583$ nm of ASTM Type 1 water.	47
Table 3-7: The filtration efficiency of 0.1 μ m latex beads by each sheet.....	48
Table 3-8: Triplicate filtration efficiency study with R2B pulp for method validation.....	49
Table 3-9: Summary of 300 nm filtration efficiency results determined using fluorescence spectroscopy.	50
Table 3-10: Fit Factors obtained from the Porta Count 8038 on a mannequin wearing a 3M 6000 series reusable respirator.	51

List of Abbreviations

Bleached Softwood Kraft Pulp (BSWK)
Choline chloride: glycerol (CG)
Choline chloride: oxalic acid dihydrate (CO)
Choline chloride: urea (CU)
Corona Virus Disease 2019 (COVID-19)
Deep Eutectic Solvent (DES)
Dust/Mist (DM)
Dust/Fume/Mist (DFM)
Enzymatic Mild Acidolysis Lignin (EMAL)
Healthcare Worker (HCWs)
Hydrogen-Bond Acceptors (HBAs)
Hydrogen-Bond Donors (HBDs)
Line 1 Latency (L1LAT)
Line 2 Latency (L2LAT)
Machine Chest 6 (MC6)
Microfiltration System (MFS)
Mild Acidolysis Lignin (MAL)
Milled Wood Lignin (MWL)
National Institute for Occupational Safety and Health (NIOSH)
Personal Protective Equipment (PPE)
Reject 1 Blowline (R1B)
Reject 2 Blowline (R2B)
Screen Press Discharge (SPD)
Severe Acute Respiratory Syndrome Corona Virus 2 (SARS-CoV-2)
Single Stranded RNA (ssRNA)
Thermomechanical Pulp (TMP)
Twin Wire Press 4 (TWP)
World Health Organization (WHO)

Chapter 1: Introduction

1.1 Research Goal

The purpose of this research project was to create an N95 mask from Nova Scotian softwood thermomechanical pulp. This project will determine if a wood pulp mask based prototype can be produced with a filtration efficiency comparable to that of commercial N95 respiratory masks. The Corona Virus Disease 2019 (COVID-19) pandemic has led to shortages in personal protective equipment (PPE) around the world.¹ Finding new renewable resources to rapidly and sustainably meet the demand for PPE is crucial to protecting frontline health care workers (HCWs). Additionally, this work will support the local pulp and paper industry with a new potential revenue stream. Our partner company, Port Hawkesbury Paper, is an environmentally conscious paper mill in Port Hawkesbury, Nova Scotia.

1.2 Introduction

As of June 1st, 2020 there were 6.14 million diagnosed cases of COVID-19 internationally.² By November 27, 2020, this number grew rapidly to 60.53 million cases worldwide.³ The number of cumulative cases of COVID-19 in Canada is shown below in Figure 1-1. The World Health Organization (WHO) has labeled the COVID-19 outbreak as a global pandemic. Seasonal flu outbreaks are considered epidemics because they effect one region; an epidemic becomes a pandemic once the outbreak spreads to multiple countries. COVID-19 is a respiratory disease caused by Severe Acute Respiratory Syndrome Corona Virus 2 (SARS-CoV-2). Viruses are frequently spread in the air within 0.1-0.3 μm diameter respiratory droplets that become aerosolized through coughing.⁴

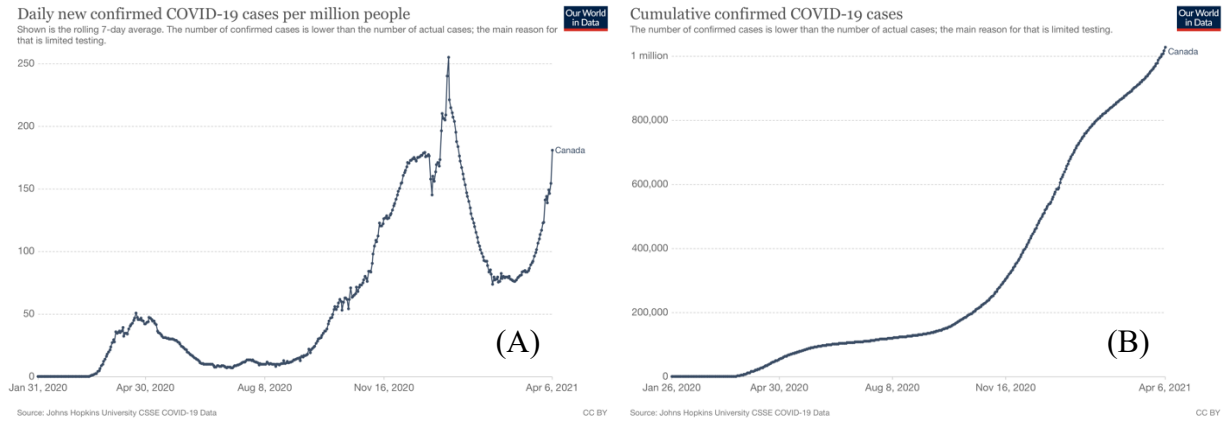


Figure 1-1: The cumulative Canadian COVID-19 case data showing (A) the number of daily new confirmed cases per million people and (B) the number of cumulative confirmed cases. Image reproduced with permission from Rosser *et al.* 2021.⁵

1.3 Literature Review

1.3.1 Viruses

Viruses are non-living infectious agents made up nucleic acid enclosed within a protein coat that are sometimes encapsulated by an envelope (Figure 1-2). This envelope is a modified form of the host's cell membrane. Viruses are able to reproduce once they are within living host cells through the lytic cycle. SARS-CoV-2 is an enveloped single stranded RNA (ssRNA) virus with spike glycoproteins protruding from the envelope.

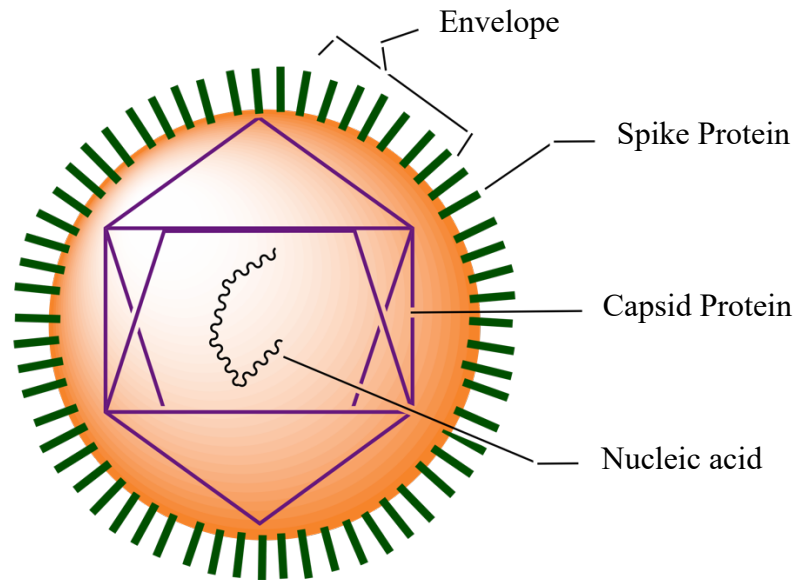


Figure 1-2: Diagram of the basic components of an enveloped virus.

In a healthcare facility there is a high risk of viral exposure. The reported detectible concentration of viruses in a healthcare facility is 12 to 16 virions/L air. An average person under a normal workload breathes at a flow rate of 32 L/min, therefore a typical healthcare worker is at risk of inhaling between 23040-30720 virions per hour.⁴

In the initial months of the COVID-19 pandemic, Guan *et al.* studied a group of 1099 patients with confirmed COVID-19 diagnoses from December 2019 to January 29, 2020.⁶ Based on the study of these patients they were able to determine some of the key clinical characteristics of the novel coronavirus. It was found that the median age of infected patients was 47 years old, with 41.9 % being female. An infected patient is said to have reached the primary composite end point when they require treatment in the intensive care unit (ICU), medical ventilation, or they die. Of the 1099 patients studied, 67 or 6.1 % of them reached the primary composite end point.⁶

1.3.2 Masks

There are many different types of masks with varying filtration efficiencies. The purpose of a mask is to limit the spread of biological aerosols. N95 masks were once certified with aerosolized

NaCl at a flow rate of 32 L/min, representative of average human breathing under normal working conditions, but as of 1995 the National Institute for Occupational Safety and Health (NIOSH) changed this certification to require NaCl to pass through the mask at a flow rate of 85 L/min, representative of average human breathing under heavy working conditions, known as 42 CFR Part 84.³ It has been found by Qian *et al.* that filtration efficiency decreases with increasing flow rate (Figure 1-3).⁸ Filters require a pressure drop; a higher pressure drop can give a higher filtration efficiency. Unfortunately, as pressure drop increases wearer comfort decreases, and therefore the optimum filter requires an ideal compromise between pressure drop and comfort.⁹

In order to be classified as an N95 mask, it must sustain a particle count filtration efficiency of 95% at the most penetrating particle size, within 0.1 μm to 0.3 μm , of aerosolized sodium chloride with a total filter loading of up to 200 mg.⁸ The filtration efficiency of a mask is known to decrease as particle size decreases down to 300 nm, after which the filtration efficiency increases with decreasing particle size. This observation is due to a change in the particle capturing mechanism of filtration taking place for various particle sizes. Larger particles are captured by the filter using impaction and interception, whereas smaller particles are captured based on Brownian diffusion.⁹ The most penetrating particle size ranges from 0.1 μm to 0.3 μm as a result of these differences in capture mechanisms.

Qian *et al.* compared the filtration efficiency of three different (>95%) N95 respirators to the less efficient (82%) dust/mist (DM), (92%) dust/fume/mist (DFM) respirators, and (71%) noncertified surgical masks.⁸ Overall, surgical masks and other alternatives to N95 masks are not sufficient to provide complete protection against nanometer-size bioaerosols.¹⁰

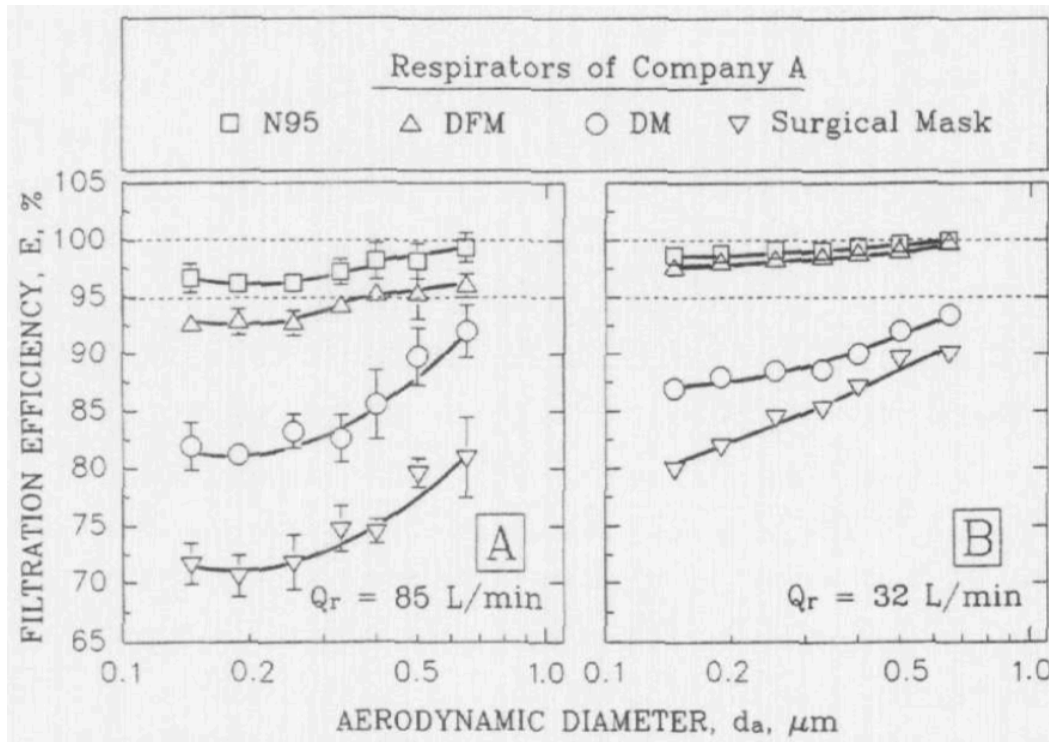


Figure 1-3: Comparison of filtration efficiencies of four mask types including N95, Dust/Fume/Mist (DFM), Dust/Mist (DM) and surgical measured at a flow rate of (A) 85 L/min and (B) 32 L/min. Image reproduced with permission from *Qian et al.*⁸

One of the main complaints of people who are required to wear N95 masks for prolonged periods of time is low breathability, disrupting their respiratory and dermal mechanisms.¹¹ There are some features added to masks to increase wearer comfort and breathability such as adjustable ear loops, malleable nose wires, and micro-ventilation fans. It should be noted that micro-ventilation fans increase wearer comfort by rapidly removing unfiltered carbon dioxide from the dead space between the mask and the wearer's face.¹¹ N95 masks are required to only have one way filtration which protects the wearer from the external environment, but not the external environment from the wearer. One way filtration utilizes a check valve that opens when the wearer exhales and closes when the wearer inhales.¹²

1.3.3 Wood Pulp and Papermaking

Trees are made up of plant tissues known as sclerenchyma. The plant cells within the sclerenchyma tissue contain rigid cell walls composed of three main components: cellulose, hemicellulose, and lignin.¹³ Cellulose is considered to be the most abundant natural polymer on earth. The structure of cellulose consists of $\beta(1,4)$ linked D-anhydroglucopyranose sugar units (Figure 1-4).¹⁴ Hemicellulose is the second most abundant polymer in plant cell walls and is similar to cellulose, but is a heteropolysaccharide with a lower degree of polymerization than cellulose.¹⁴ Instead of glucose, hemicellulose is made up of sugars such as mannose and galactose.¹⁵ Lignin is an aromatic polymer. Lignin is used as a matrix for polysaccharide components within plant cell walls. The presence of lignin was needed in the evolution of terrestrial plants because of its ability to make plant cell walls rigid and hydrophobic, therefore lignin gave plants the ability to retain water on land.¹⁶ Lignin is responsible for holding wood fibers tightly together which makes paper brittle. Lignin is oxidized photochemically which can be seen when old newspapers have yellow fading.¹⁵

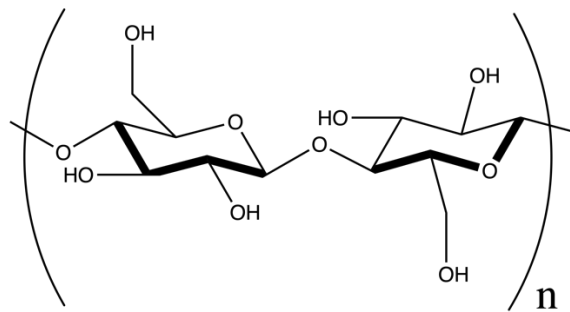


Figure 1-4: The chemical structure of cellulose.

Paper making involves several key steps: pulping, the removal of cellulose from most of the hemicellulose, lignin, oils, waxes and minerals; beating and refining, increasing surface area by fibrillation of cell walls; wet-end papermaking, and draining off the water from the cellulose

fibers.¹⁵ Wood pulp is composed of spirally wound cellulose fibers that form the hierarchical structure of a wood fiber (Figure 1-5). Fibrillation of cell walls involves mechanical beating to separate fibers, therefore increasing the overall surface area. Increased surface area results in greater particle capture ability.⁹ Wood pulp fibrillation experiences an issue called hornification, where fibrillation in the wet state collapses and re-bonds when air dried.⁹

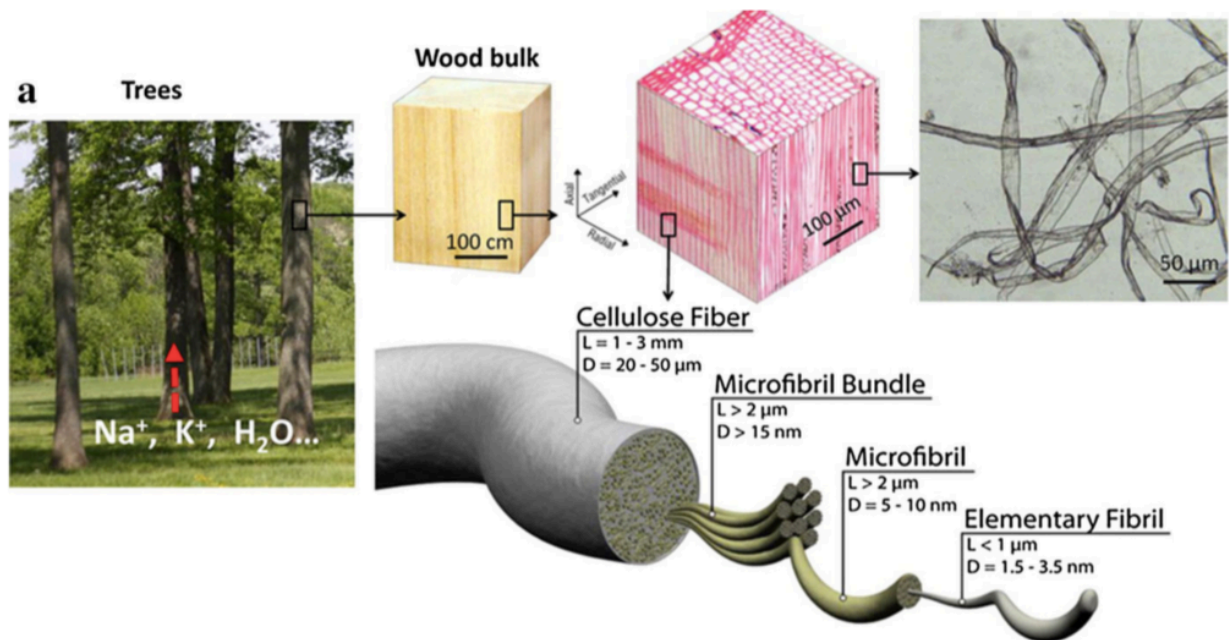


Figure 1-5: A scheme depicting the hierarchical structure of a wood fiber. Image reproduced with permission from *Zhu et al.*¹⁷

Port Hawkesbury Paper produces a thermomechanical bleached softwood pulp. Softwoods have longer fibers than hardwoods; long fibers allow for more fibrillation because of greater abrasion in the mechanical beating phase.⁹ Port Hawkesbury Paper’s pulp is ideal, because it is processed in a more environmentally friendly way than alternative Kraft pulps.

1.3.4 Cellulose Based Filtration

This work is novel, because there has been no previous account in the literature of a 100% wood pulp N95 respirator being constructed. One group has previously shown that a Kraft softwood pulp was able to filter at an efficiency and pressure drop comparable to N95 masks.⁹ Kraft pulp is produced in a basic chemical pulping process, whereas thermomechanical pulp is produced in a high energy mechanical process. The hypothesis of this thesis research is that a similar efficiency can be achieved with a non-Kraft pulp. One known drawback of using paper based materials for producing masks in this work is wetting, rendering the mask ineffective.⁹ The method that produced the most effective product for Mao *et al.* consisted of wet beating the pulp as an initial mechanical treatment, followed by wet sheet forming (16 mm thick), and finally, freeze drying in situ to avoid hornification.⁹ Hornification is the formation of hydrogen bonds between fibrillated pulp fibers resulting in loss of fibrillation when pulp goes from the wet to the dry state.

Metreveli *et al.* used fluorescence to test nanocellulose based filters from filamentous green algae, *Cladophora algae*.¹⁸ Filamentous algae was selected as a cellulose source because it has the advantage of not undergoing the process of hornification. This nanocellulose based filter was found to filter at an equivalent efficiency compared to the industrially available synthetic polymer based filters currently used.

At present, wood pulp is only used in the comfort layers of masks but not as the actual filtering material. Harmac Pacific is an example of a Canadian pulp mill that currently supplies medical pulp to external companies for use in personal protective equipment production. Harmac Pacific produces a Bleached Softwood Kraft Pulp (BSWK). In particular, one of these BSWK products originates from softwood Western red cedar trees. One drawback of the use of Western red cedar in PPE is that it is a contact allergen.¹⁹ In contrast, Port Hawkesbury Paper produces a

thermal mechanical pulp (TMP). TMP is a softwood pulp which originates from Balsam Fir and Black Spruce. Subramanian *et al.* summarize compositional differences between kraft pulp and TMP which are organized below in Table 1-1.²⁰

Table 1-1: Comparison of Kraft Pulp to TMP.²⁰

Kraft Pulp	TMP
Higher [Cellulose]	Lower [Cellulose]
Lower [Lignin]	Higher [Lignin]
Higher [Na ⁺ , Mg ²⁺ , Fe ²⁺]	Higher [K ⁺ , Ca ²⁺ , Mn ²⁺]
Higher [Water]	Lower [Water]
Less Dense	More Dense

There are many organizations that regulate wood pulp standards. In Canada the regulatory organization for wood pulp testing is the Pulp and Paper Technical Association of Canada (PAPTAC). Whereas, in the United States the regulatory institution is the Technical Association of the Pulp and Paper Industry (TAPPI).

1.3.5 Lignin

Lignin is an aromatic polymer that acts like “glue” holding together wood fibers and providing pulp with good compressibility. Lignin undergoes photooxidation, therefore prolonged exposure to light causes fading in the coloration of paper products. Additionally, paper that has a high lignin content is more brittle.¹⁵ Lignin is an amorphous aromatic polymer that varies in exact structure based upon the plant species being analyzed, an example of a proposed structure of one type of softwood lignin is shown in Figure 1-6. One advantage to removing lignin from pulp used for mask production is that lignin decreases the naturally high water vapor transmission of wood pulp.²¹ Fabric breathability is determined by a materials ability to dissipate thermal energy to the surroundings by water vapor transmission.²² Therefore, the removal of lignin would increase the breathability of wood pulp as a material for mask production.

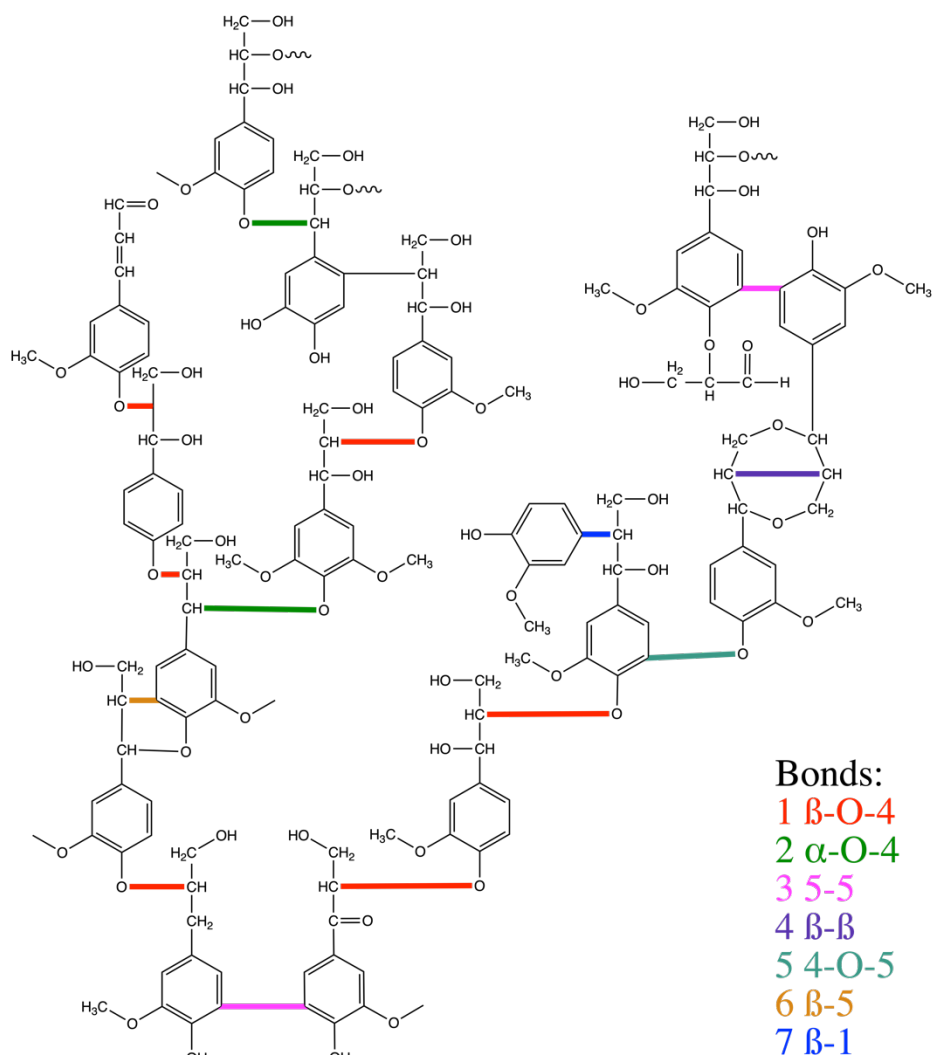


Figure 1-6: The main bond linkages present in softwood lignin. Image adapted from Laurichesse *et al.*²³ Bolded bonds are included to clearly indicate the lignin linkages.

Although the structure of lignin varies by plant species, all lignin is composed of the same precursor monolignols (Figure 1-7).²³ The functional groups and bonds present in each monolignol can be used for planning out chemical reactions in the pulping process. The monolignols are connected together through carbon-carbon and ether linkages, specifically alkyl-aryl ether linkages. Approximately 12 monolignols are linked together to form the structure of lignin.²³ Softwood lignin is mainly made up of guaiacyl units and a small amount of p-hydroxyphenyl units.²³

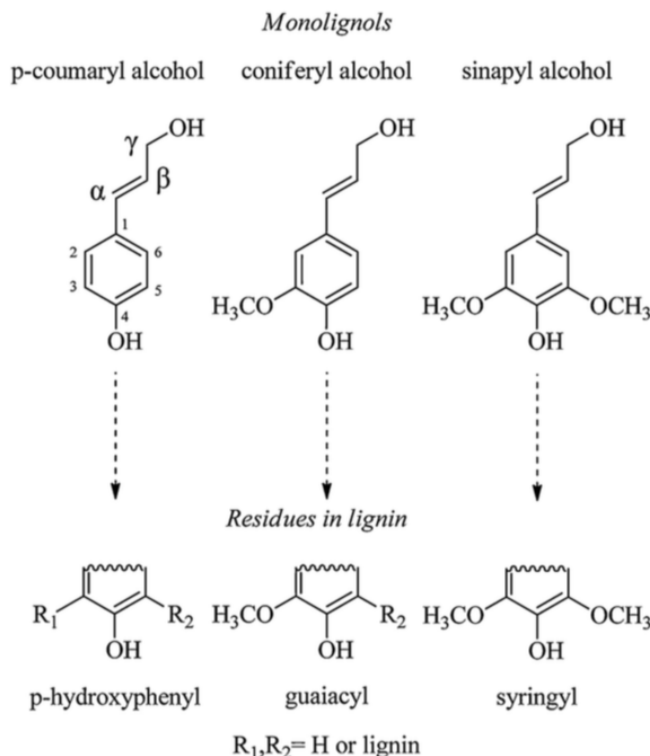


Figure 1-7: The three monolignol precursors and their structures within lignin polymers. Image reproduced with permission from Laurichesse *et al.*²³

The key difference between the pulp produced at Port Hawkesbury Paper, and the pulp used to test filtration efficiencies comparable to N95 masks was that those filters were manufactured by a kraft process.⁹ Kraft pulping uses black liquor, a solution of aqueous sodium hydroxide and sodium sulfide, to solubilize the lignin and hemicellulose present in the pulp.²⁴ The liquor depolymerizes the lignin by cleavage of the aryl ether bonds.²⁴ The structure of dissolved and residual lignin is further modified by condensation reactions forming carbon-carbon bonds. The reason why Port Hawkesbury Paper uses a thermomechanical process instead of the kraft process is because the kraft process has a harsh impact on the environment due to an effluent rich in sodium salts and calcium salts.

Presently, there are other methods for lignin extraction from pulp that are broken down into analytical scale processes and industrial scale processes. Some examples of analytical scale

processes include: milled wood lignin (MWL) where some aryl ether linkages are cleaved in a ball mill and then the product is extracted by 1,4-dioxane; mild acidolysis lignin (MAL) where wood chips are ball milled and then treated with cellulolytic and hemicellulolytic enzymes; and enzymatic mild acidolysis lignin (EMAL) which is a method combining enzymatic and acid hydrolysis.²⁴ There are also many current industrial processes that are used for separating wood components: the kraft process as described above; lignosulfonates (LS) process using bisulfite; soda lignin (SL) where lignin is dissolved by an alkaline solution without any sulfur; and organosolv lignin (OSL) where organic solvents and acids are used for solubilizing and degrading the lignin.²⁴

Lignin is hydrophobic and its presence is hypothesized to decrease interfiber bonding of wood pulp.²⁵ Interfiber bonding is an important variable because it positively correlates with paper strength.²⁶ Increased paper strength is advantageous in producing more durable PPE. Some lignin must be removed to increase interfiber bonding but not all of it, because lignin is a large contributor to the pulp's bulk mass. By only removing some of the lignin the end processing yields are much larger.²⁵ The presence of surface lignin can be seen through scanning electron microscopy (SEM) as debris on the fibers.²⁵ Overall, the removal of lignin is a goal of this thesis research because decreasing lignin content correlates with increasing breathability and paper strength.

In addition to SEM, lignin content can be determined indirectly by oxidation with potassium permanganate, via a procedure known as the Kappa number determination.²⁷ The presence of lignin can be determined qualitatively by methods such as infrared spectroscopy and UV-Vis spectroscopy.^{28,29} NMR spectroscopy can also be used for quantitative analysis of lignin content, but its application is limited in this case because the lignin region has been observed to have considerable peak overlap.²⁹

1.3.6 Deep Eutectic Solvents

Deep eutectic solvents (DES) are prepared by mixing together two or more solid components in the correct proportion resulting in a substance with a lower melting point than either individual component. This correct proportion is known as the eutectic point. Deep eutectic solvents are gaining in popularity because they require a small amount of energy consumption to be produced, are synthesized in high yields, are environmentally friendly, and result in a thermally stable solvent.³⁰ DES are produced using a known molar ratio of hydrogen-bond acceptors (HBAs) and hydrogen-bond donors (HBDs).³¹ In a choline chloride: urea DES, for example choline chloride acts as the HBA and urea acts as the HBD. Another popular HBD is lactic acid, which can be used in a choline chloride: lactic acid 9:1 ratio. The choline chloride: urea DES interaction is proposed by Ashworth *et al* to occur with a eutectic point at a 1:2 ratio, as shown below in Figure 1-8.³²

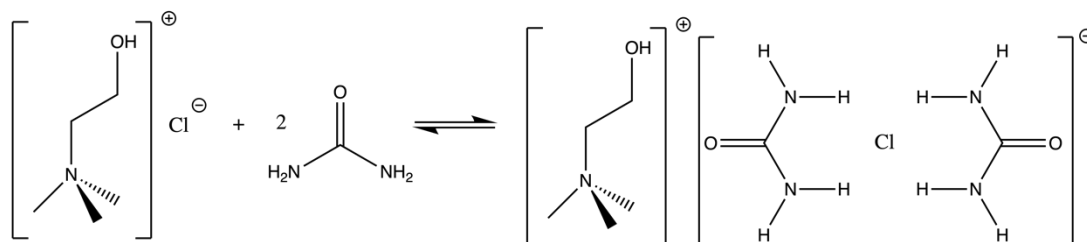


Figure 1-8: The proposed choline chloride: urea DES interaction with an eutectic point at a 1:2 ratio. Image adapted from Ashworth *et al.*³²

Wang *et al.* propose that the choline chloride: oxalic acid DES interaction involves an exchangeable proton as depicted in Figure 1-9.³³ Within this interaction oxalic acid is acting as the HBD. The choline chloride: oxalic acid DES eutectic temperature is around 60°C.³³ A series of common DES, their molar ratios, and melting points are provided below in Table 1-2.³⁴

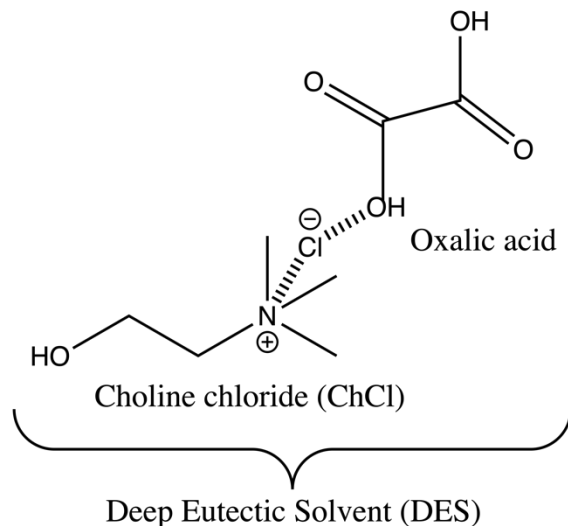


Figure 1-9: Choline chloride: oxalic acid DES interaction. Image adapted from Wang *et al.*³³

Table 1-2: Common DES molar ratios and melting points. Table adapted from Tang and Row.³⁴

DESs	Salt:HBD (molar ratio)	Melting point (°C)
ChCl-Urea	1:2	12
ChCl-benzamide	1:2	92
ChCl-imidazole	3:7	56
ChCl-adipic acid	1:1	85
ChCl-benzoic acid	1:1	95
ChCl-citric acid	1:1	69
ChCl-oxalic acid	1:1	34
ChCl-phenylacetic acid	1:1	25

Yu *et al.* analyzed the impact of three different DES pre-treatments on the production of cellulose nanofibrils from raw ramie fibers.³⁵ Ramie is a flowering plant that grows in eastern Asia. Specifically, the three DES analyzed included choline chloride: urea (CU), choline chloride: oxalic acid dihydrate (CO), and choline chloride: glycerol (CG). The impact of these treatments on the ramie fibers was characterized by SEM analysis. CO pre-treatment was found to result in the most dramatic changes in ramie fibers of the three DES treatments used. This dramatic change in the

ramie fibers is attributed to CO being able to effectively remove amorphous cellulose and noncellulosic components from the fiber. The non-cellulosic components removed included hemicellulose, water solubles, pectin, and lignin.

1.3.7 Kappa Number

Kappa number is a technique used heavily in the wood pulp industry for quantifying and comparing the acid soluble lignin content of various biomass samples. In this method the lignin content is indirectly detected by the reduction of potassium permanganate and reoxidation of lignin resulting in a calculated “kappa number” output.²⁷ One limitation of Kappa number quantification of lignin is that the relationship between the kappa number and the content of lignin varies for each specific pulp based on the way that it has been refined and the bleaching processed it has been exposed to. Additionally, Kappa number determination is time consuming and requires daily standardization of reagents for the titration to produce accurate results. The Kappa number technique remains a standard procedure in the wood pulp industry because it is one of the only simple quantitative options for determining lignin content.

1.3.8 Fluorescence Spectroscopy

Metreveli *et al.* fabricated cellulose based filter membranes and tested their filtration efficiency with fluorescence spectroscopy.¹⁸ These membranes were prepared by sonicating *Cladophora* algae, dispersing the algae in water, draining water off of the sample with a nylon filter, and subsequently drying the cellulose based filter on a heat press. The fluorospectrophotometric profiles were scanned for all samples. Initially, a blank pure solvent (water) was analyzed. Subsequently, a standard start solution containing a fluorophore with a known concentration was analyzed. Lastly, the filtrate following filtration with the nanocellulose filter the fluorospectrophotometric profile was measured. The fluorophores used in these studies

were sulfate-modified polystyrene fluorescent beads that were either 30 nm, 100 nm, or 500 nm (Figure 1-10). This nanocellulose based filter was found to be able to filter at an equivalent efficiency of the industrially available polymer based filters currently used for virus removal.¹⁸

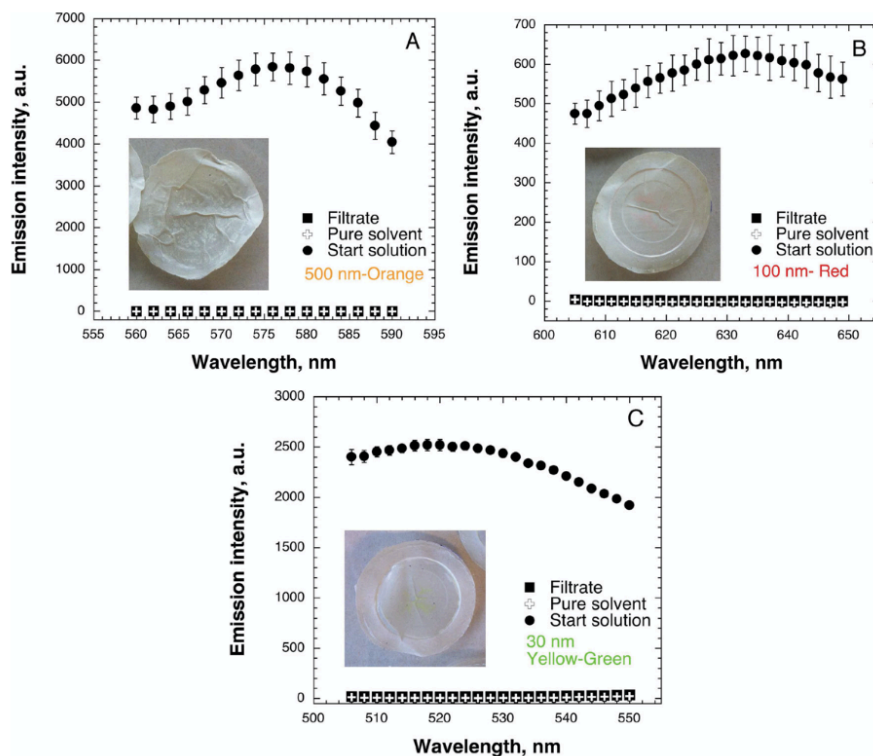


Figure 1-10: The fluorospectrophotometric profiles measured for of the blank pure solvent, the start solution containing the fluorophore, and the filtrate following filtration with the nanocellulose. The size of fluorescent beads used for each experiment varied (a) 500 nm, (b) 100 nm, and (c) 30 nm. Each results is the average of three measurements. The photograph inlet on each plot is the *Cladophora* membranes following the filtration. Image reproduced with permission from *Metreveli et al.*¹⁸

1.3.9 Aerosol Testing

NIOSH utilizes aerosol testing to certify N95 masks.⁷ Aerosol testing chambers can be quite elaborate in the instrumentation they require and can be costly. This method remains the standard for mask certification because it simulates the conditions of filtering out small particulates in the air without introducing interfering variables such as filter wetting. Recently, in light of the shortages of personal protective equipment caused by the COVID-19 pandemic, Schilling *et al.*

designed an accessible and rapid aerosol filtration method for comparison of the filtration efficiency of various types of masks.³⁶ This rapid method does not replace NIOSH testing but simply allows for an affordable option for the comparison of multiple masks quickly. This method could be applied in early stage prototyping of a new mask design to demonstrate which material has the most potential to move into NIOSH testing. The schematic of the instrumental set-up for the rapid aerosol testing method and an example of its data output is shown below in Figure 1-11.

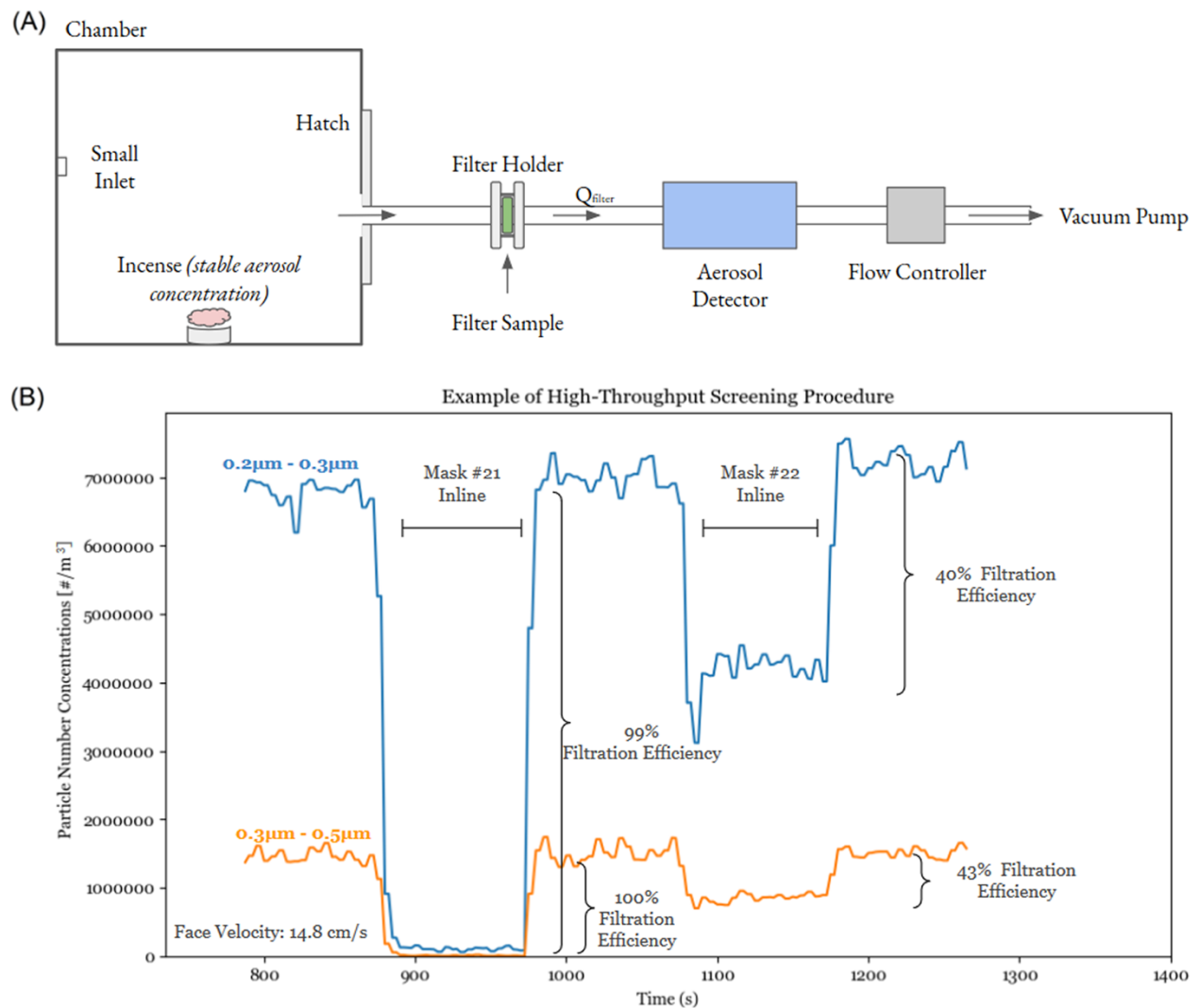


Figure 1-11: The (a) schematic of the instrumentation required for the rapid aerosol testing method and (b) the data output received from this experimental set-up. Image reproduced with permission from Schilling *et al.*³⁶

Additionally, other research groups have also been working on developing simplified experimental set-ups for testing fit factors and filtration of aerosols through masks worn by mannequin heads, such as Faridi *et al.* whose experimental set up is shown below in Figure 1-12.³⁷ Faridi *et al.* used two separate identical experimental set-ups and compared results with and without a respirator face mask present on the dummy head. This group used a flow rate of 16 L min⁻¹ pulled by a vacuum pump to draw in aerosols from the outside air into a mixing chamber where these aerosol particles could be detected by an aerosol spectrometer.

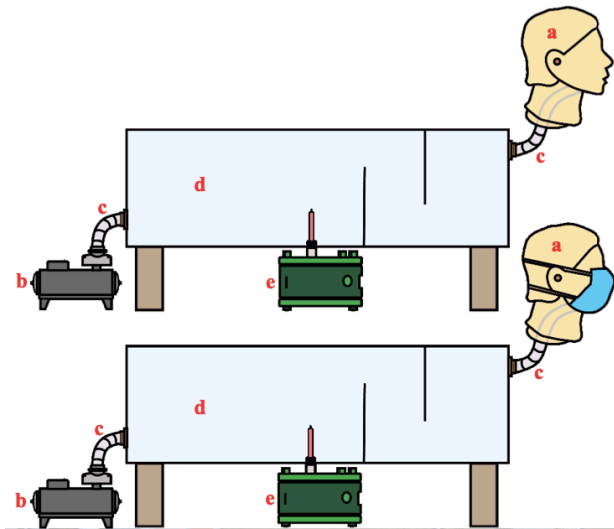


Figure 1-12: Experimental set-up to test mask aerosol filtration. Where (a) is a mannequin head, (b) is a vacuum pump, (c) is tubing, (d) is a sealing mixing chamber, and (e) is a GRIMM Aerosol Spectrometer. Imaged reproduced from Faridi *et al.*³⁷

A fit test is used to rapidly evaluate how adjusting the fit of a respirator can impact its filtration efficiency. During the fit testing of a certified series 100/99/95/P1/P2/P3/HEPA mask, all penetration detected is assumed to only occur due to face-seal leakage and not filter penetration. The PortaCount provides a quantitative output known as a fit factor. The fit factor is the sum of the face seal leakage and the filter penetration. In this thesis work the face-seal leakage is assumed to be low due to the use of a small respirator tightly adjusted to a mannequin head.

1.4 Theory

1.4.1 Wood Pulping

Kraft pulping is one of the most well-known industrial processes for the removal of lignin. The Kraft process relies on a lignin hydrolysis reaction in which a cleavage of the β -O-4 aryl ether linkages in lignin occurs (Figure 1-13).³⁸ Kraft pulping uses black liquor, a solution of aqueous sodium hydroxide and sodium sulfide, to solubilize the lignin and hemicellulose present in the pulp.²⁴ The liquor depolymerizes the lignin by cleavage of the aryl ether bonds.²⁴ The structure of dissolved and residual lignin is further modified by condensation reactions forming carbon-carbon bonds.

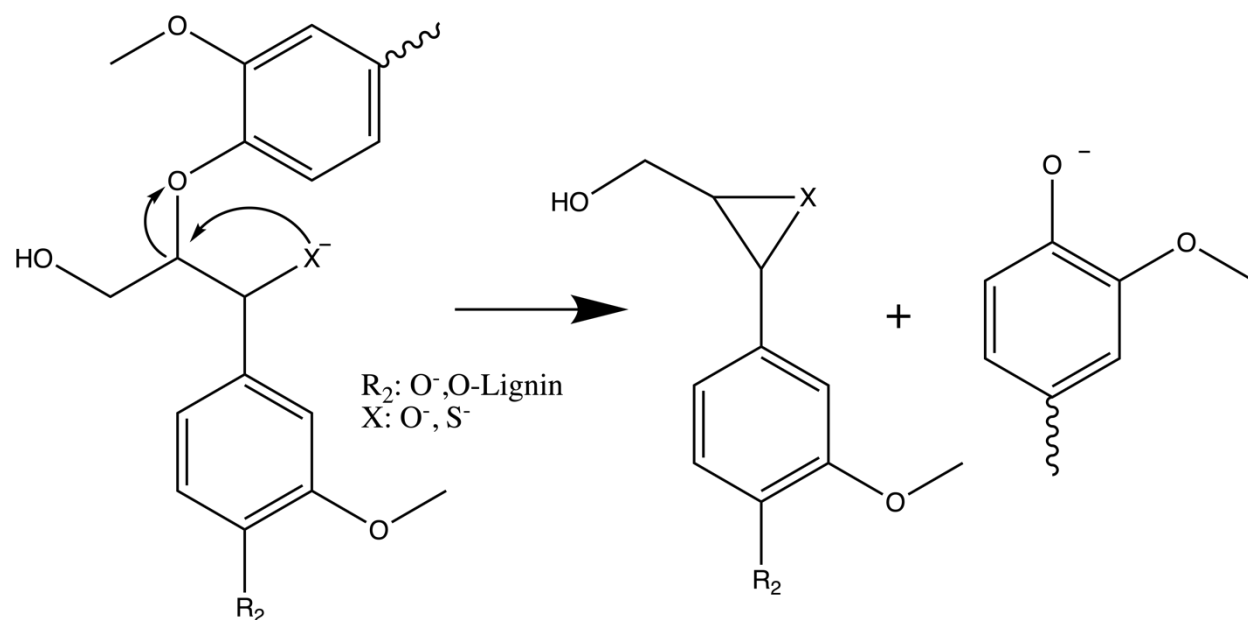


Figure 1-13: Kraft cleavage of β -O-4 aryl ether linkages in lignin. Image adapted from Froass *et al.*³⁸

1.4.2 Spectroscopic Methods for Lignin Detection

Lignin content within a wood pulp sample has been reported to be characterized by infrared spectroscopy (IR) analysis.²⁸ One limitation of IR methods when compared to other lignin characterization techniques, such as the Kappa number titration, is that IR is only a qualitative

technique. Additionally, ultraviolet visible spectroscopy (UV-Vis) can be used to analyze aqueous lignin content.³⁹ Lignin is a photosensitive molecule that develops a yellow color through oxidation resulting in a UV-Vis peak observed at 280 nm.⁴⁰ UV-Vis analysis is advantageous because it requires simple instrumentation that is available at a low cost but its qualitative analysis is limited due to the subtle lignin absorption. Nuclear magnetic resonance (NMR) spectroscopy is a quantitative technique that can be used for lignin analysis due to its ability to provide detailed structural information. NMR is not a common candidate for lignin analysis, however, because the lignin region in NMR has been reported to have a considerable amount of peak overlap.²⁹ Additionally, NMR is less sensitive and more expensive than other lignin characterization techniques.

1.4.3 Deep Eutectic Solvents

Deep eutectic solvents are synthesized by mixing together the correct molar ratio of two or more solid components such that the eutectic point is reached. The eutectic point is the composition at which the two components form a substance with a lower melting point. The concept of the eutectic point is illustrated in Figure 1-14 with a simple phase diagram. DES are made such that they contain large asymmetric ions which allow for lower melting points due to decreases in lattice energy. The lattice energy is synonymous with the strength of the bonds within an ionic compound. The presence of choline chloride in the DES increases the β -O-4 cleavage rate within the delignification process of wood pulp.⁴¹

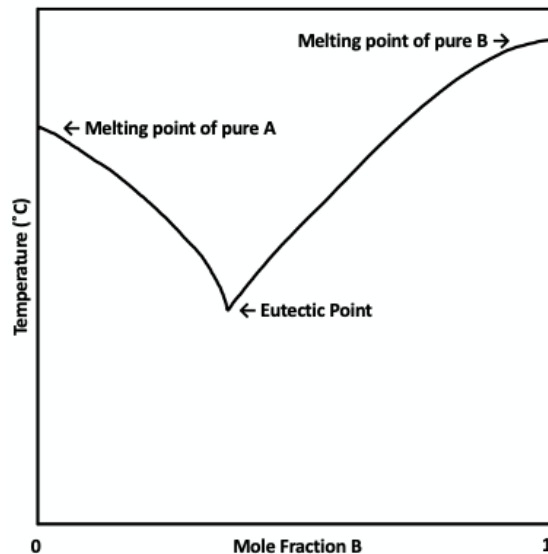
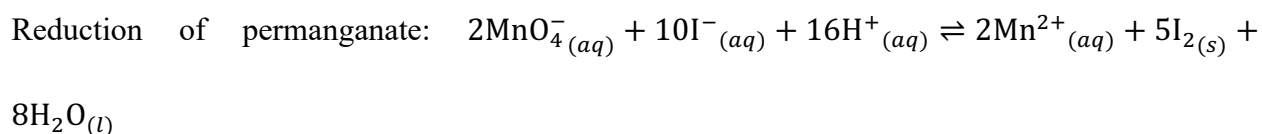


Figure 1-14: The phase diagram showing the eutectic point for a specific composition of components A and B.

1.4.4 Kappa Number

Kappa number is a quantitative factor used in the pulp and paper industry to compare lignin content of various pulp samples. Permanganate has many possible oxidation states including 7+, 2+, 6+, and 4+. In the Kappa Number reaction, permanganate in the 7+ oxidation state is reduced by acidified potassium iodide to give the 2+ oxidation state and a pale pink solution. At a 50% consumption rate only 3 of the 5 electrons needed for this redox reaction are transferred, visually this gives a brown solution. Permanganate oxidation degrades the aromatic rings in lignin by addition of the permanganate to all of the double bonds giving ring rupture. Mechanistically, this procedure utilizes a stepwise reduction of potassium permanganate followed by the oxidation of lignin and carbohydrates.⁴² The reactions of the kappa number titration are summarized in Scheme 1-1. Additionally, the equation used to calculate the Kappa Number is shown in Equation 1-1.



Liberated iodine titrated with thiosulfate: $I_{2(s)} + 2S_2O_3^{2-}{}_{(aq)} \rightleftharpoons 2I^-{}_{(aq)} + S_4O_6^{2-}{}_{(aq)}$

Permanganate consumption: $3e^- + MnO_4^-{}_{(aq)} + 4H^+{}_{(aq)} \rightleftharpoons MnO_{2(s)} + 2H_2O_{(l)}$

Scheme 1-1: The reaction occurring during the Kappa Number titration.

Equation 1-1: Calculating Kappa Number.⁴²

$$K = \frac{p \times f}{w} \quad \text{and} \quad p = \frac{(b-a)N}{0.1}$$

Where:

K = Kappa Number

f = correction for 50% permanganate consumption

w = weight of dried pulp (g)

p = 0.1 N permanganate consumed (mL)

b = thiosulfate consumed in blank (mL)

a = thiosulfate consumed by test specimen (mL)

N = normality of thiosulfate

The change in Kappa Number, ΔK , is calculated by finding the difference between the Kappa Number for the untreated pulp and the Kappa Number for the treated pulp. A negative value for ΔK indicates that there is a decrease in the lignin content. The percentage of insoluble lignin in pulp can be approximated to be 13% of the kappa number.⁴²

1.4.5 Fluorescence

When an electron absorbs electromagnetic radiation it is excited to a higher energy level. Fluorescence occurs when energy is emitted, releasing a photon while the electron moves from the excited to ground state. Fluorescence competes with non-radiative processes such as vibrational relaxation and internal conversion. As a result of this competing energy loss fluorescence is often represented as the emission intensity over a range of wavelengths. Vibrational relaxation is when vibrationally excited molecules transfer their excess energy to molecules within the surrounding solvent. Vibrational relaxation leaves the molecule in the lowest vibrational state within an excited

electronic state. Internal conversion is when energy is transferred from a species in the lowest vibrational level of an excited electronic state to the surrounding solvent molecules, resulting in the movement of the excited species to the lower electronic state. All of the changes in energy described in absorption, fluorescence and non-radiative processes are depicted in Figure 1-15.⁴³

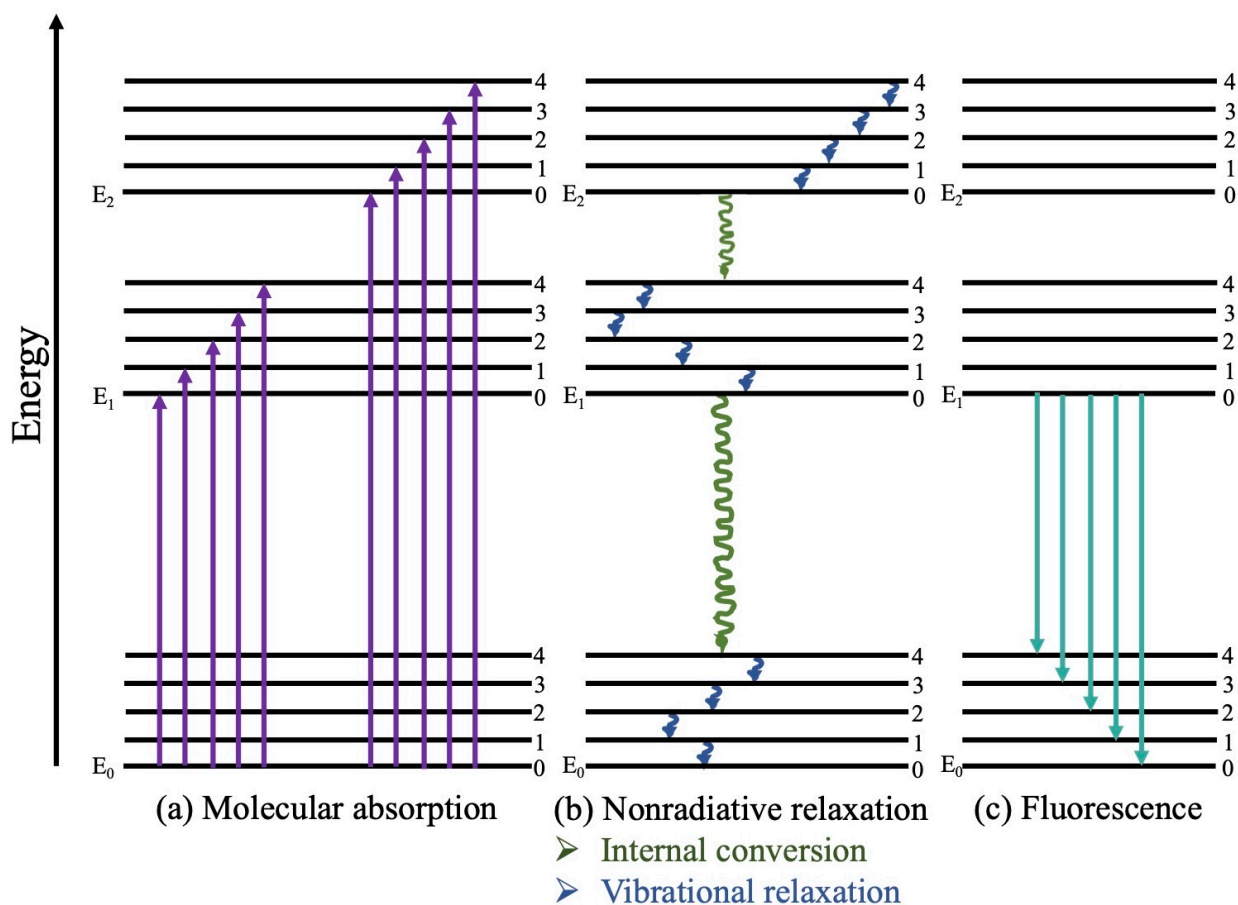


Figure 1-15: The energy level diagram represents the changes in electronic state in (a) molecular absorption, (b) nonradiative relaxation, and (c) fluorescence. Image adapted from Skoog *et al.*⁴³

1.4.6 Aerosol Testing

Penetration during the fit test of a respirator is considered to have two sources: filter penetration and face-seal leakage. The PortaCount uses a condensation nuclear counter to detect the difference in concentration of particles inside (C_{in}) and outside (C_{out}) of a filtering face respirator.⁴⁴ The fit factor is reported as the ratio of C_{out}/C_{in} . The PortaCount works by using a

minimally penetrating particle size for fit test measurements such that filter penetration becomes negligible and only face-seal leakage is recorded.

The N95-Companion is an electrostatic classifier that is designed to be used in conjunction with the PortaCount for fit testing N95 filtering-facepiece respirators. The N95-companion is used to select particles within the 30 – 60 nm range to not penetrate the N95 filter material, but instead to be passed on to the PortaCount. The use of the N95 companion is essential for determining the fit factor of N95 masks, because the electrostatic filter material used in N95 masks is reported to make the most penetrating particle size range fall in-between 40 – 60 nm for aerosol testing.⁴⁵ Therefore, because of this shift in the most penetrating particle size fit factors obtained for N95 masks are biased based on the invalid assumption. The most penetrating particle size (MPPS) is under debate because it varies based on electrostatic charge. The MPPS for fibrous filters is 300 nm, whereas the MPPS for electrostatic filter material is 40 – 60 nm. The MPPS is also impacted by flow rate and particle charge. Overall, this means that fit factors obtained without the use of the N95-companion must include both face-seal leakage and filter penetration in the variables contributing to lower fit factors.⁴⁵

The 8026 particle generator is a controlled particle generator, as opposed to more traditional particle generating techniques, such as burning a candle. The particle generator ensures that the ambient aerosol concentration stays at 70 particles/cc by generating a sodium chloride aerosol.⁴⁶

Chapter 2: Experimental

2.1 Sheet Forming

TAPPI standard 205 specifies the requirements for forming handsheets for the physical testing of pulp. This project did not have access to a sheet machine or disintegrator, therefore in place of a disintegrator a blender (high, 30 seconds) was used to disintegrate pulp into ASTM Type 1 water (solution resistivity $\geq 18.2 \text{ M}\Omega \text{ cm}$, 946 mL). In place of a sheet machine a paper forming screen on top of a support grid was placed into a vat of ASTM Type 1 water. The blended pulp was poured directly onto the paper forming screen. The pulp was manually mixed to ensure even distribution of the fibers on the paper forming screen. Once fibers were evenly distributed on the screen, the screen was lifted straight out of the water and held flat to allow water to drain (15 seconds), subsequently the screen was held at a 45° angle and more water was allowed to drain off of the screen (15 seconds).

Water was sponged off of the paper sheet through a second cover screen until no further water could be removed. The second cover screen was removed and replaced with a Scott Heavy Duty Shop Towel. The paper screen was then removed and the shop towel was folded over both sides of the paper sheet. The folded shop towel was then placed on a heat press machine (BetterSub Heat Press 12x15 Inch Combo 5 in 1 Heat Press Machine, BetterSub Store) at $110^\circ\text{C} \pm 8^\circ\text{C}$ for 5 minutes. The shop towel was then removed from the heat press. A digital caliper was used to measure the thickness of 20 spots on the newly formed paper sheet. The paper sheets were then cut into 0.30 mm diameter filter paper to be used for filtration studies. A flow chart of the paper sheet forming process summarizing all steps is shown below in Figure 2-1.

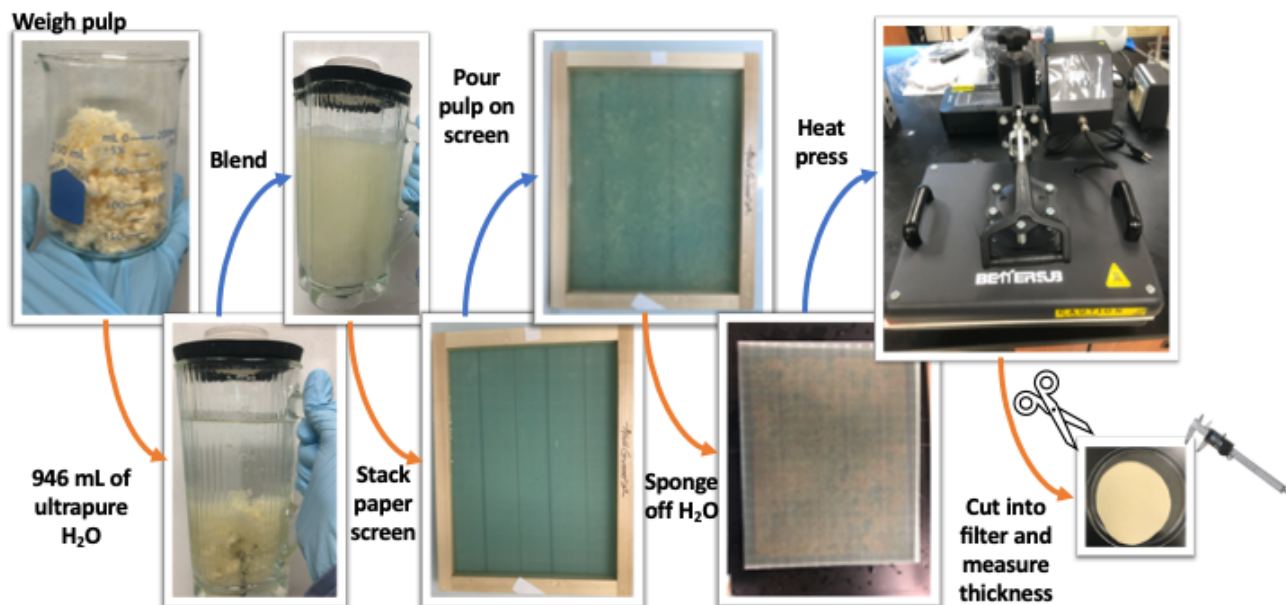


Figure 2-1: Flow chart of the paper sheet forming process.

2.2 Kappa Number

Kappa number testing requires that reagents be accurately and precisely prepared as well as standardized such that potassium permanganate is 0.1000 ± 0.0005 N, sodium thiosulfate is 0.2000 ± 0.0005 N, and potassium iodide is 0.1 N. This standardization is required because the concentration of reagents impacts the Kappa number calculation. All reagents must be kept at exactly $25 \pm 0.5^\circ\text{C}$ throughout the reaction. The starting weight of the pulp varies but must be accurately known in order to account for this variation in Kappa number calculation. Prior to Kappa number determination pulp samples were dried in an oven at 60°C for 1 hour followed by 20 minutes in a desiccator. Kappa number was determined according to the TAPPI/ ANTSI T 236, OM 13 test method.⁴⁷ Throughout the Kappa number reaction sulfuric acid is used to reduce permanganate, which competes with the rapid oxidation reaction between lignin and permanganate, this reduction of permanganate gives a dark purple color. After exactly 10 minutes iodine was used to quench the reaction giving a red color. The solution was then titrated with

thiosulfate to reach a yellow color. Finally, a starch indicator was added and the solution was titrated to a colorless endpoint. The number of replicates performed was dependent upon the yield of pulp following modification.

2.3 Infrared Spectroscopy

An attenuated total reflection infrared (ATR-FTIR) spectrometer (Bruker, Massachusetts) was used to collect all IR spectra. All spectra were baseline corrected using Bruker OPUS software. An ATR-FTIR with a diamond crystal was used for all recorded measurements and 32 scans were taken for each measurement.

2.4 Deep Eutectic Solvent

Deep eutectic solvents were used as a treatment to remove lignin from the TMP. Three different deep eutectic solvents were used for pulp treatment. Each reaction had a specific molar ratio, reaction temperature, reaction time, pulp drying treatment, and potential rehydration step (following pulp drying, the pulp was sometimes rehydrated with a known amount of water). All reaction conditions corresponding to each reaction code explored in this thesis are summarized below in Table 2-1.

Table 2-1: DES Reaction Conditions.

DES (molar ratio)	Experimental Code	Rxn Temperature (°C)	Rxn Time (hr)	Dried (Y/N)	Rehydration (Y/N)
Choline chloride: oxalic acid dihydrate (1:1)	DES-01-R2B	100	2	N	N
Choline chloride: oxalic acid dihydrate (1:1)	DES-02-R2B	60	2	N	N
Choline chloride: oxalic acid dihydrate (1:1)	DES-03-R2B	90	2	N	N
Choline chloride: oxalic acid dihydrate (1:1)	DES-04-R2B	100	2	Y	N
Choline chloride: oxalic acid dihydrate (1:1)	DES-05-R2B	100	2	Y	Y (8.0 g)
Choline chloride: oxalic acid dihydrate (1:1)	DES-06-R2B	100	2	Y	Y (3.0 g)
Choline chloride: oxalic acid dihydrate (1:1)	DES-07-A-R2B	70	3	Y	N
Choline chloride: oxalic acid dihydrate (1:1)	DES-07-B-R2B	65-70	3	Y	N
Choline chloride: oxalic acid dihydrate (1:1)	DES-08-R2B	100	2	Y	Y (2.4 g)
Choline chloride: urea (1:2)	DES-09-R2B	140	6	Y	N
Choline chloride: urea (1:2)	DES-10-L1LAT	140	10	Y	N
Choline chloride: urea (1:2)	DES-11-L1LAT	140	6	Y	N
Choline chloride: urea (1:2)	DES-12-L1LAT	100	6	Y	N
Choline chloride: urea (1:2)	DES-13-L1LAT	80	6	Y	N
Choline chloride: urea (1:2)	DES-14-A-L1LAT	80	1	Y	N
Choline chloride: urea (1:2)	DES-14-B-L1LAT	80	1	Y	N
Choline chloride: urea (1:2)	DES-15	80	6	Y	N
Choline chloride: lactic acid (9:1)	DES-16	80	4	Y	N

2.5 Fluorescence Testing

Latex beads coated in sulfate-modified polystyrene, 100 nm (L9902; 2.5% solids; red; $\lambda_{ex} \approx 538$ nm; $\lambda_{em} \approx 584$ nm, Sigma Aldrich) were used for the 100 nm fluorescence studies. Polystyrene beads, carboxylate-modified, 300 nm (93470720011150; 1% solids; white; $\lambda_{ex} \approx 333$ nm; $\lambda_{em} \approx 613$ nm, Thermo Fisher Scientific) were used for 300 nm fluorescence studies. All fluorescent bead suspensions were prepared using ASTM Type 1 water (solution resistivity ≥ 18.2 M Ω cm).

Fluorescence measurements were recorded using a Cary Eclipse Fluorescence Spectrophotometer. The spectrophotometer was blank corrected first with ASTM Type 1 water. Measurements were recorded 10 times and are reported as the average of 10 simple reads. The fluorophore suspensions were filtered through a vacuum microfiltration system (MFS) with a handmade paper sheet filter. The difference in fluorescence reading of the suspension prior to and following filtration was used to calculate the filtration efficiency of each test paper sheet (Equation 2-1). There were no rinsing steps in this process.

$$\text{Filtration Efficiency} = \frac{(a - b)}{a} \times 100 \%$$

a = Fluorescence intensity of the fluorophore suspension

b = Fluorescence intensity of the fluorophore suspension following filtration

Equation 2-1: The filtration efficiency of the paper material.

2.6 Mannequin Head Aerosol Test

A hole was cut through the mouth of a rubber mannequin head (BNP Lashes) for a PVC tube. The PVC tubing (I.D. x O.D. ¼ in x 3/8 in) was connected to a vacuum pressure station

(Barnant Company). Subsequently, the mannequin head was fit with a small 3M™ 6000 series half face mask respirator (179869A). 3M™ Reusable Respirator Accessory Filter Adapters (19070324) fit onto each side of the respirator. These filter adapters hold 3M™ N95 particulate filters (18-999-4547) with the help of the 3M™ 6000 Series Respirator Accessory, Filter Retainer 501 (17673B). The mannequin head aerosol test set-up is shown below in Figure 2-2. A PortaCount (8038, TSI, St. Paul, Minn.) was used for all aerosolized particle detection. A 8026 particle generator was used to generate enough aerosols within a small enclosed room to allow for proper aerosol detection.



Figure 2-2: The mannequin head set up for aerosol testing.

2.7 Scanning Election Microscopy Studies

Pulp and paper sheets were imaged before and after DES treatment using a TESCAN MIRA 3 LMU Variable Pressure Schottky Field Emission Scanning Electron Microscope (FE-SEM). The FE-SEM has a maximum resolution of 1.2 nm at 30 kV. Paper sheets were air dried for at least 24 hours prior to imaging. All samples were prepared on carbon tape and gold coated to reduce charging. Following analysis, SEM image processing for characteristics such as fiber width was completed using with ImageJ software (NIH, Maryland, USA).

Chapter 3: Results and Discussion

3.1 Characterization of Commercial Personal Protective Equipment

Personal protective equipment was obtained and analyzed to gain a better understanding of how medical and non-medical grade fabrics are currently produced. The 3M N95 mask was analyzed as a NIOSH certified three layer N95 mask. This mask consists of an outer layer that protects the mask from humidity in the outside environment, the middle layer is the active filter layer, and the inner layer is closest to the wearer's face protecting the filter from moisture. The inner layer limits moisture transmission from the wearer's mouth so that the filtration efficiency of the middle layer is not impacted. The mask and scanning electron microscopy (SEM) image of the filter layer are shown below in Figure 3-1.

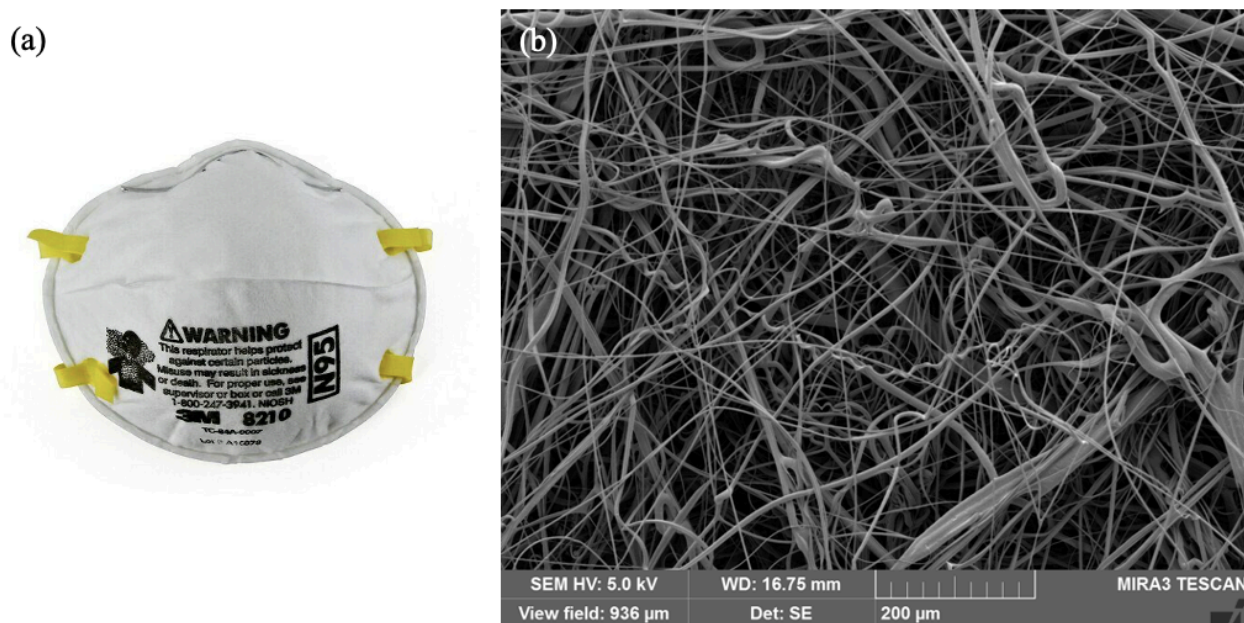


Figure 3-1: (a) The 3M brand N95 mask. The 3M mask is a NIOSH certified three layer N95 mask. (b) The SEM image of the middle filter layer of the 3M mask. SEM (voltage: 5.0 keV, Det: SE, Tescan MIRA3 LMU Field Emission SEM).

ATR-FTIR was used to analyze the mask layers of the 3M N95 mask (Figure 3-2). The second layer is the proposed filter layer, Image J analysis of 20 fibers within the filter layer gave an average width of $3.5 \mu\text{m} \pm 1.7 \mu\text{m}$. Based off of comparison of the ATR-FTIR spectra of each

mask layer to literature spectra it is suspected that the filter layer is composed of polypropylene and the inner and outer layer are polyester.^{48,49}

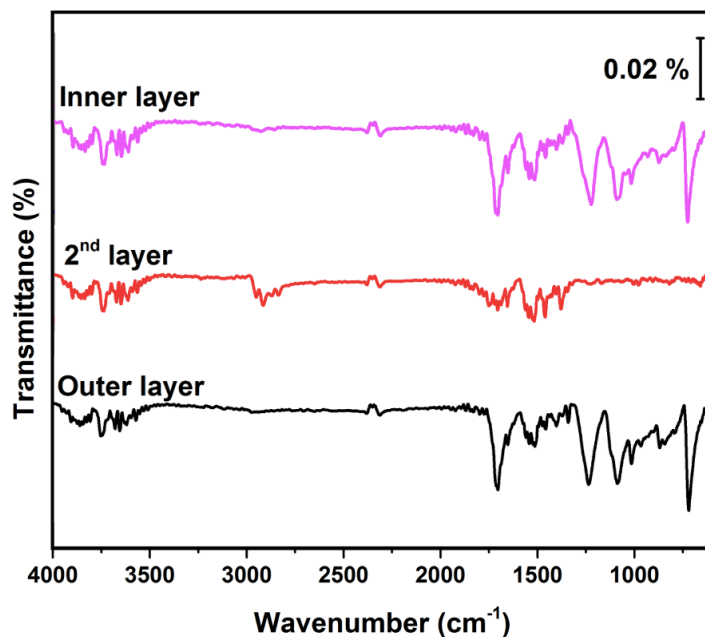


Figure 3-2: The FTIR spectra of the three layers of the 3M N95 mask.

The DEGiL NIOSH certified N95 mask was analyzed under SEM (Figure 3-3). Image J analysis of 20 fibers within this mask's filter layer resulted in an average fiber width of $5.1 \mu\text{m} \pm 2.9 \mu\text{m}$. All three layers of this mask were further analyzed by ATR-FTIR (Figure 3-4). Based on comparison of the ATR-FTIR spectra obtained to literature spectra it is suspected that the inner and filter layers of the DEGiL mask are composed of polypropylene and that the outer layer is made up of polyester.^{48,49}

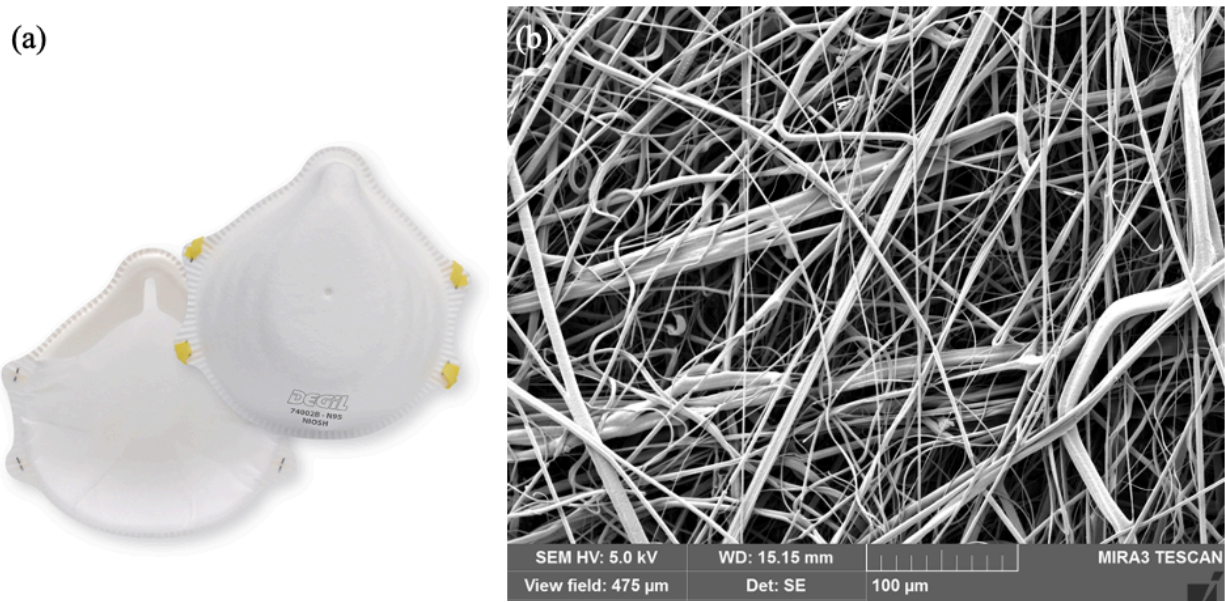


Figure 3-3: (a) The DEGiL brand N95 mask. The DEGiL mask is a NIOSH certified three layer N95 mask. (b) The SEM image of the middle filter layer of the DEGiL mask. SEM (voltage: 5.0 keV, Det: SE, Tescan MIRA3 LMU Field Emission SEM).

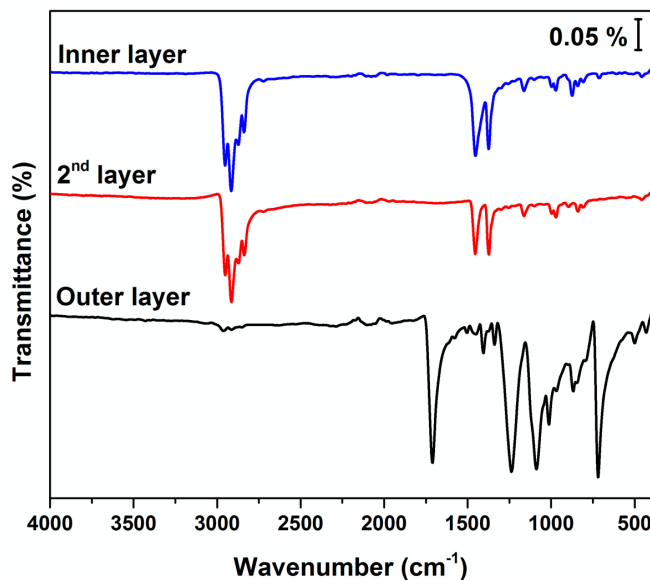


Figure 3-4: The ATR-FTIR spectra of the three layers that compose the DEGiL N95 mask.

The InterMask^(TM) 3 Ply Disposable Face Mask was analyzed by SEM (Figure 3-5). Image J analysis of 20 fibers within the filter layer gave an average width of $5.1 \mu\text{m} \pm 4.0 \mu\text{m}$. An ATR-FTIR spectrum was recorded for each of the three layers that make up the InterMask^(TM) 3 Ply

Disposable Face Mask (Figure 3-6). Based upon comparison of the ATR-FTIR spectra to literature values it is suspected that all three layers of this mask are mainly composed of polypropylene.⁴⁸

(a)

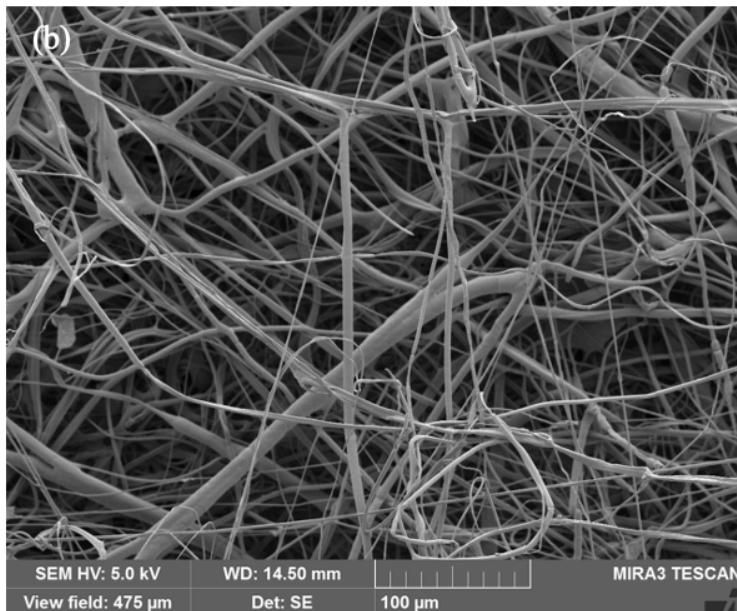


Figure 3-5: (a) The InterMask^(TM) 3 Ply Disposable Face Mask. (b) The SEM image of the middle filter layer of the InterMask^(TM) 3 Ply Disposable Face Mask. SEM (voltage: 5.0 keV, Det: SE, Tescan MIRA3 LMU Field Emission SEM).

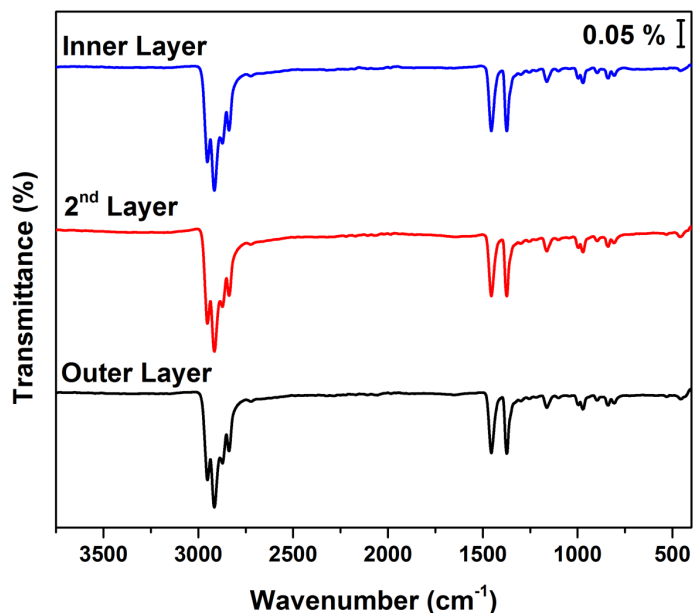


Figure 3-6: The ATR-FTIR spectra of the three layers that compose the InterMask^(TM) 3 Ply Disposable Face Mask.

Further characterization of non-woven medical fabrics included a comparison of the SEM appearance of the fabrics used to make isolation gowns as well as the outer layers of the 3M N95 mask, the DEGiL N95 mask, and the InterMask^(TM) 3 Ply Disposable Face Mask (Figure 3-7). Image J analysis showed that the isolation gown material had an average fiber width of $23.0 \mu\text{m} \pm 3.9 \mu\text{m}$ for the 20 fibers measured.

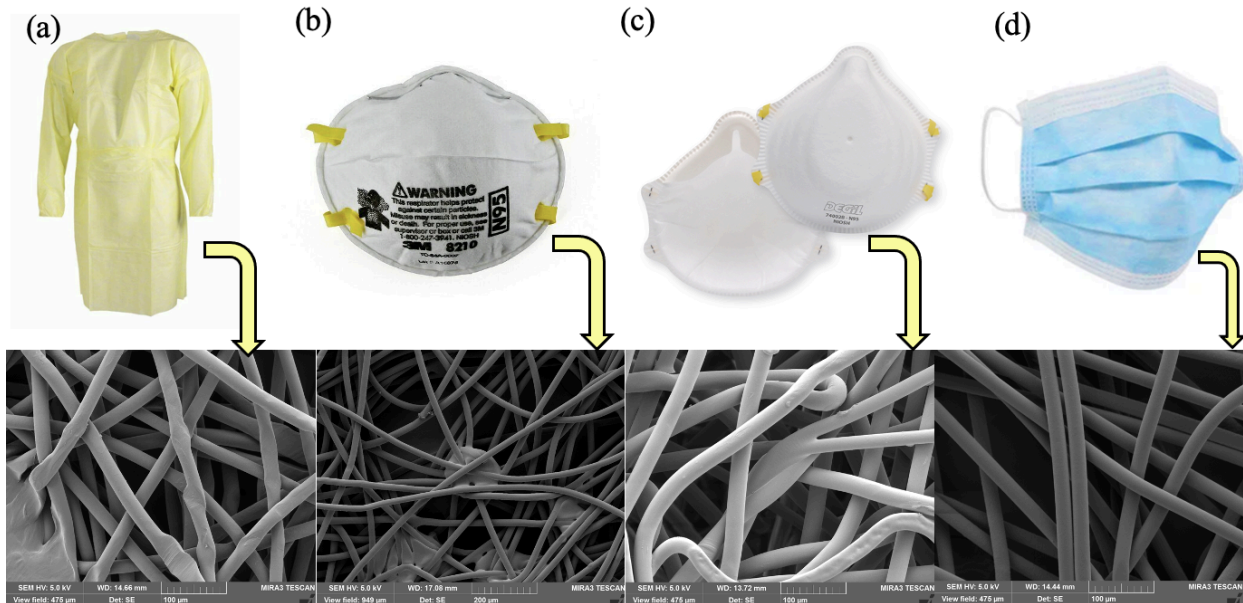


Figure 3-7: SEM characterization of the outer fabric layer of various personal protective equipment including (a) a disposable isolation gown, (b) the 3M N95 mask, (c) the DEGiL N95 mask, and the InterMask^(TM) 3 Ply Disposable Face Mask. SEM (voltage: 5.0 keV, Det: SE, Tescan MIRA3 LMU Field Emission SEM).

Ahlstrom Monksjo is a supplier of fabrics that are used in the production of personal protective equipment. Currently two of the outer mask support layer fabrics they offer, DRAPE Wetlaid and DRAPE Sterilization Economy Plus, are both made of cellulose based materials. SEM images of these materials are shown below in Figure 3-8. The fibers of these two different fabrics appear similar in morphology. ATR-FTIR analysis of both fabric samples gave all of the same peaks so only one of these two spectra is shown below in Figure 3-9.

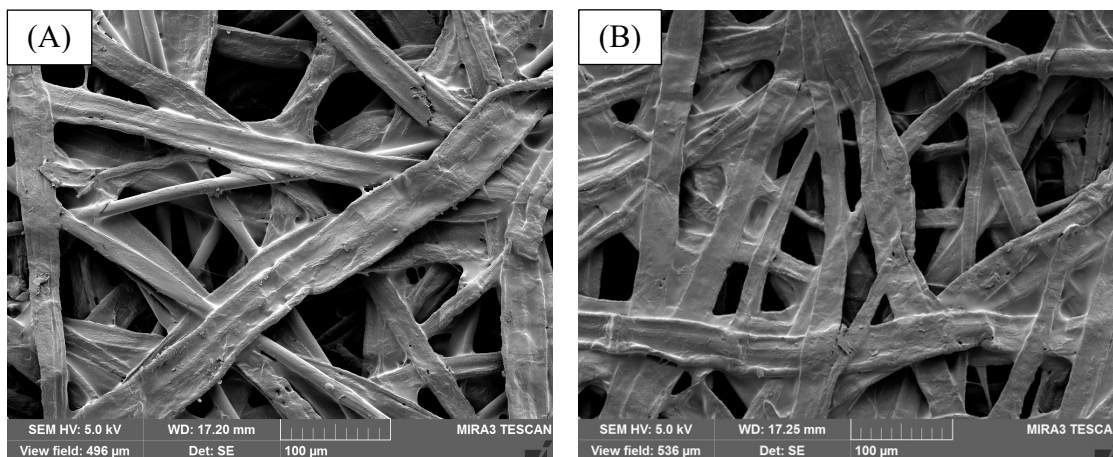


Figure 3-8: Cellulose based mask support layer distributed by Ahlstrom Monksjo. Including (a) DRAPE Wetlaid and (b) DRAPE Sterilization Economy Plus.

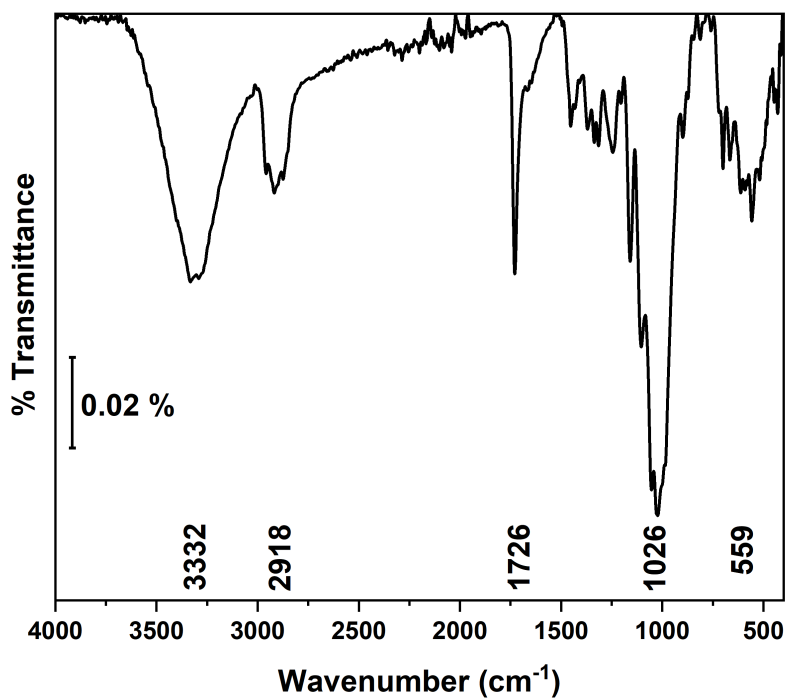


Figure 3-9: FTIR of DRAPE Wetlaid Ahlstrom Monksjo Mask Support Layer fabric.

Spectral band assignments of the ATR-FTIR spectrum of DRAPE Wetlaid fabric are shown below in Table 3-1. Functional group assignments are consistent with what would be expected for cellulose. It is especially apparent that this material is cellulose based on the oxygen-

hydrogen stretching present, and this would not be expected for any of the commonly used synthetic polymers.

Table 3-1: Spectral band assignments of ATR-FTIR of DRAPE Wetlaid Ahlstrom Monksjo mask support layer fabric.

Functional Group	Observed frequency	Expected frequency range
$\nu(\text{O-H})$ in alcohols and phenols, OH stretch (solids and liquids)	3332 cm^{-1}	3420 - 3250 cm^{-1} (s)
$\nu(\text{CH}_3)$ and $\nu(\text{CH}_2)$ in aliphatic compounds, CH antisymmetric and symmetric	2918 cm^{-1}	2990 – 2850 cm^{-1} (m-s)
$\nu(\text{C=O})$ in ketone, C=O stretch	1726 cm^{-1}	1720 – 1700 cm^{-1} (s)
$\nu(\text{CH}_2\text{-OH})$ in primary alcohols, C-O stretch	1026 cm^{-1}	1060 - 1025 cm^{-1} (vs)
$\nu(\text{C-C=O})$ in ketones, C-C=O bend	559 cm^{-1}	560 – 510 cm^{-1} (s)

3.2 Characterization of Pulp Samples

Samples of Nova Scotian thermomechanical softwood pulp from Port Hawkesbury Paper are shown below in Figure 3-10. In Figure 3-11, the fiber morphology can be seen for various samples of pulp pulled from different places along the treatment line including: Reject 2 Blowline (R2B), Reject 1 Blowline (R1B), and Screw Press Discharge (SPD). Additional pulp samples include handsheets received from Port Hawkesbury paper and K10s pulp sheets from Harmac Pacific. This K10s pulp is the previously mentioned western red cedar kraft pulp. One hand sheet of untreated MC6 pulp received from Port Hawkesbury Paper can be seen as an SEM image below in Figure 3-12. MC6 pulp is unique from the other pulp samples studied because it is taken off of the production line later in the process and contains clay.

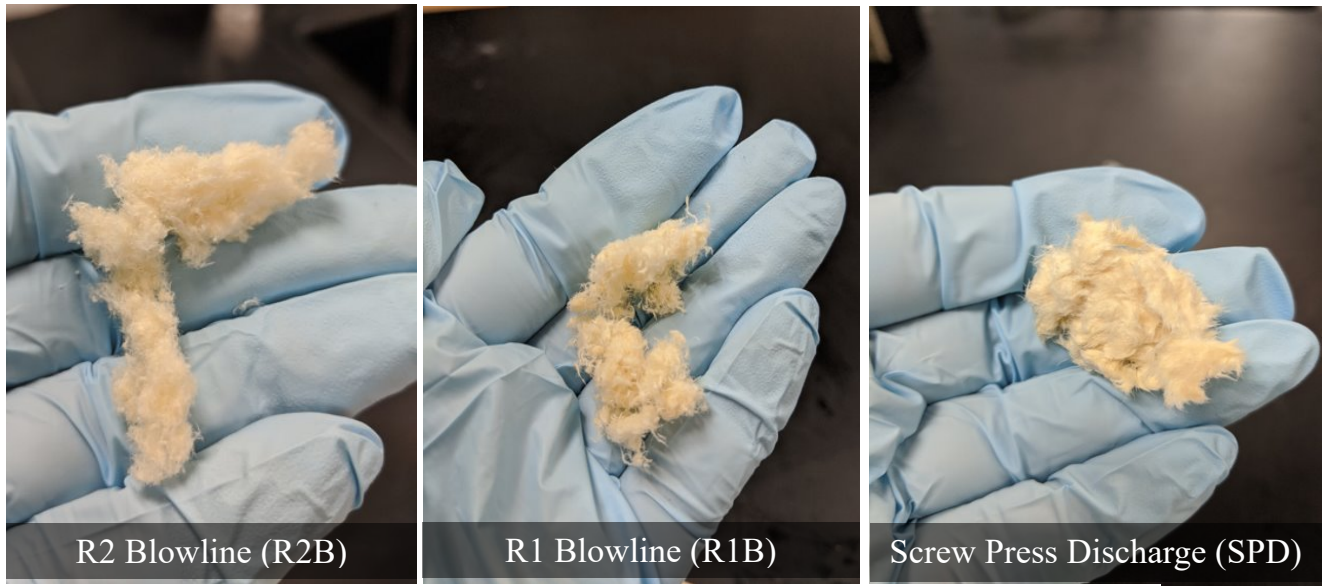


Figure 3-10: The pulp samples as received from Port Hawkesbury Paper.

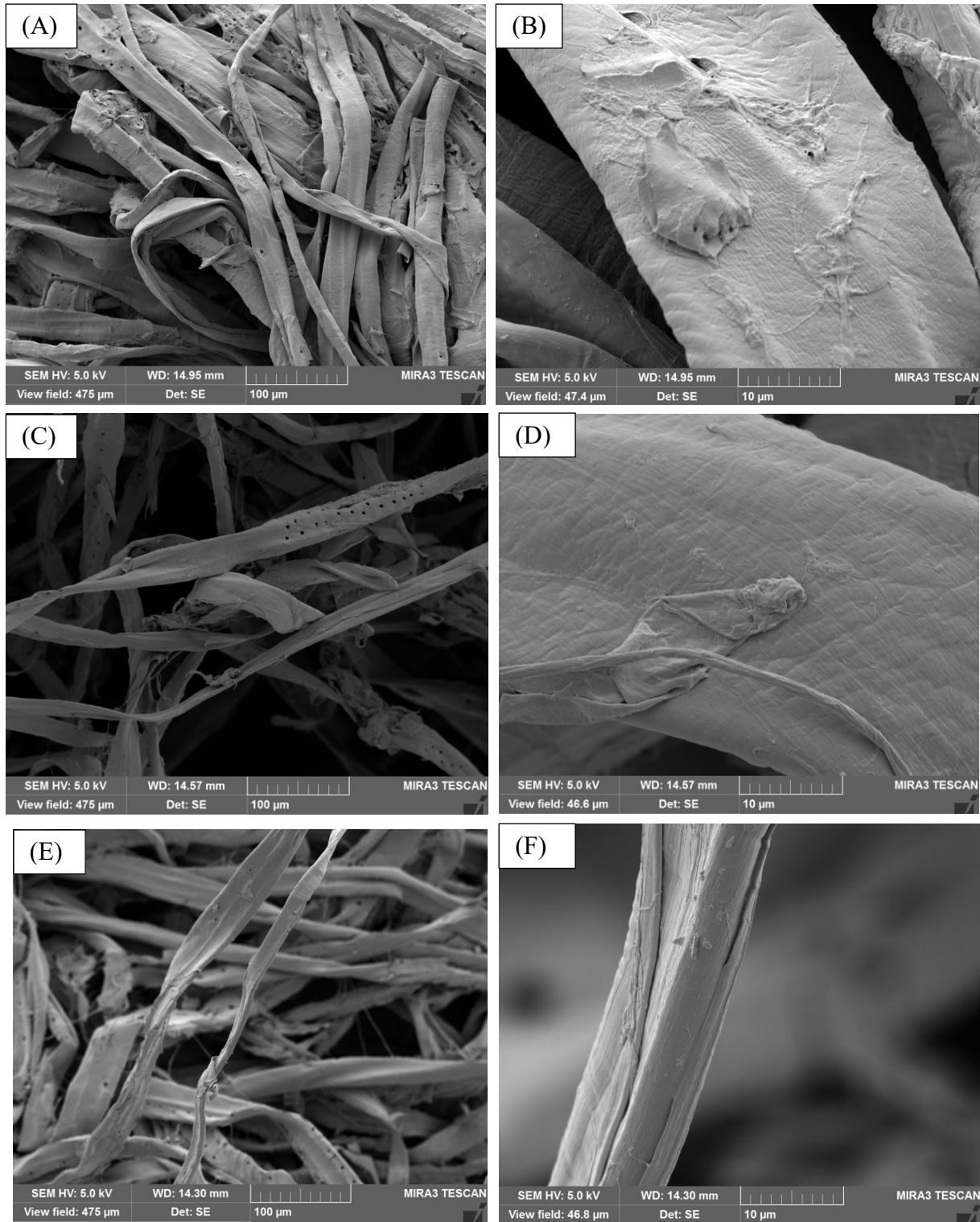


Figure 3-11: SEM Images of unmodified pulp samples (A & B) R1B, (C & D) R2B, and (E & F) SPD. SEM (voltage: 5.0 keV, Det: SE, Tescan MIRA3 LMU Field Emission SEM).

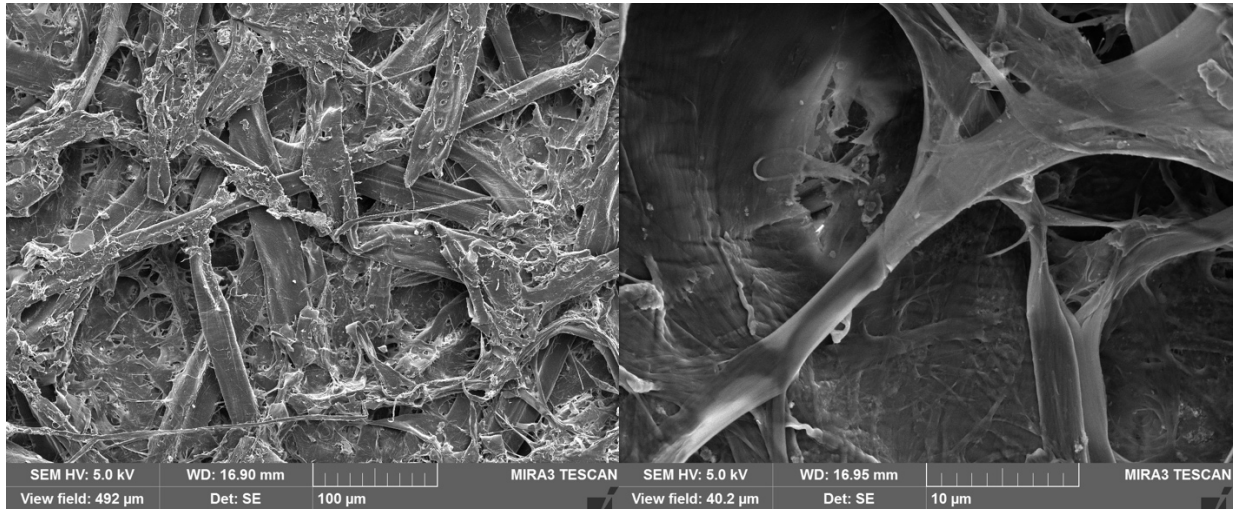


Figure 3-12: Untreated MC6 hand sheet. SEM (voltage: 5.0 keV, Det: SE, Tescan MIRA3 LMU Field Emission SEM).

SEM with Energy Dispersive X-Ray Analysis (EDX) was used to analyze the elemental composition of the carbon coated untreated MC6 hand sheet. Port Hawkesbury uses clay in the MC6 pulp which is seen in EDX as a mixture of oxygen, aluminum, and silicon across the surface. These elements are commonly found together in kaolinite. Kaolinite is a clay mineral with a chemical composition of $\text{Al}_2\text{Si}_2\text{O}_5(\text{OH})_4$. Kaolin clay is an advantageous paper additive because it increases the paper's strength and lowers the cost of manufacturing.⁵⁰

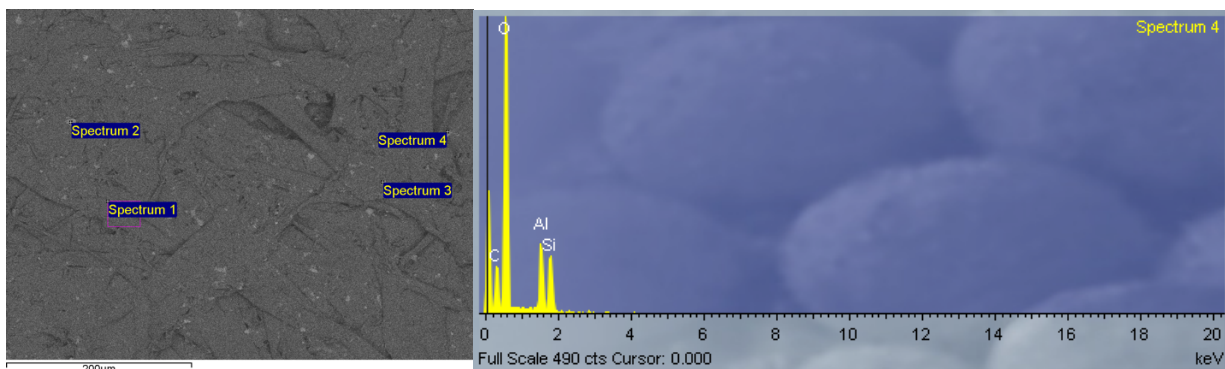


Figure 3-13: SEM-EDX analysis of an Untreated MC6 hand sheet. SEM (voltage: 5.0 keV, Det: SE, Tescan MIRA3 LMU Field Emission SEM).

Kappa Number was measured for various pulp samples to determine the insoluble lignin content. The change in Kappa number, ΔK , is reported in Table 3-2 for various treatments of R2B pulp. The more negative the ΔK value, the more lignin is removed from the sample.

Table 3-2: Kappa number results for untreated and DES treated pulps.

Experimental Code	Mass of Sample (g)	P-Value	K-Value	ΔK
Untreated R2B	0.4003	46	113.9	N/A
	0.5009	55	111.01	N/A
	0.6007	62	105.89	N/A
DES-04-R2B	0.6007	60	102.08	-3.8
DES-05-R2B	0.3024	32	101.79	-24.2
DES-06-R2B	0.6002	66	113.81	11.8
	0.3000	33	106	-17.5
DES-07-A-R2B	0.3085	46	147.7	20.8
DES-07-B-R2B	0.3013	39	126.46	3.5
Untreated L1LAT	0.408	52	127.96	N/A
Untreated L1LAT	0.5011	58	117.71	N/A
Untreated L1LAT	0.7035	69	102.2	N/A

*N/A is listed as the ΔK value of the untreated samples because ΔK is calculated based off of the K value of the untreated sample.

3.3 Deep Eutectic Treatment of Pulp Samples

Two different deep eutectic treatments have been explored throughout the course of this project (Table 3-3). Initially, the impact of a choline chloride: oxalic acid dihydrate treatment on filtration efficiency was analyzed. One major issue with this DES is that it produces a pulp so fine that nearly all of these modified pulp samples were not able to be made into paper sheets. This was because when the fibers are too small they pass directly through the paper forming screen. The choline chloride: urea DES appears to remove less lignin but is advantageous because it yields a product with fibers that can be made into paper sheets for filtration studies. The reaction conditions for each DES treatment including temperature, time, drying, and rehydration are summarized in Table 3-3.

Table 3-3: DES Reaction Yields.

DES (molar ratio)	Experimental Code	Pulp:DES	Initial Mass	Final Mass	Yield	Observations
Choline chloride: oxalic acid dihydrate (1:1)	DES-01-R2B	1:50	5.0 g	1.62 g	32.4%	Wet initial pulp (60% water content), Very fine dark brown solid.
Choline chloride: oxalic acid dihydrate (1:1)	DES-02-R2B	1:50	5.0 g	1.93 g	38.5%	Very fine dark brown solid.
Choline chloride: oxalic acid dihydrate (1:1)	DES-03-R2B	1:50	5.0 g	1.51 g	30.2%	Very fine dark brown solid.
Choline chloride: oxalic acid dihydrate (1:1)	DES-04-R2B	1:50	5.0 g	2.45 g	49.0%	Dried first, very fine dark brown solid.
Choline chloride: oxalic acid dihydrate (1:1)	DES-05-R2B	1:50	5.0 g	1.85 g	37.0%	Rehydrated with 8 g of water, some product loss
Choline chloride: oxalic acid dihydrate (1:1)	DES-06-R2B	1:50	5.0 g	1.77 g	35.5%	Rehydrated with 3g of water.
Choline chloride: oxalic acid dihydrate (1:1)	DES-07-A-R2B	1:50	5.0 g	3.75 g	75.0%	Pale yellow, compressible
Choline chloride: oxalic acid dihydrate (1:1)	DES-07-B-R2B	1:50	5.0 g	1.56 g	62.4%	Dark yellow, slightly compressible
Choline chloride: oxalic acid dihydrate (1:1)	DES-08-R2B	1:50	4.0 g	4.49 g	112.3%	Fine brown powdery solid
Choline chloride: urea (1:2)	DES-09-R2B	1:50	2.0 g	1.80 g	90.0%	Dark yellow, slightly compressible
Choline chloride: urea (1:2)	DES-10-L1LAT	1:50	4.0 g	3.26 g	81.5%	Pale yellow, slightly compressible
Choline chloride: urea (1:2)	DES-11-L1LAT	1:100	2.0 g	1.67 g	84.0%	Pale yellow, Compressible
Choline chloride: urea (1:2)	DES-12-L1LAT	1.5:100	1.5 g	1.32 g	88.0%	Pale yellow, slightly compressible

Choline chloride: urea (1:2)	DES-13-L1LAT	1.5:100	1.5 g	1.25 g	80.0%	Pale yellow, slightly compressible
Choline chloride: urea (1:2)	DES-14-A-L1LAT	1.5:100	1.5 g	1.24 g	82.7 %	Slight brown, compressible
Choline chloride: urea (1:2)	DES-14-B-L1LAT	1.5:100	1.5 g	1.19 g	79.3 %	Did not have proper mixing, light yellow, compressible
Choline chloride: urea (1:2)	DES-15-MC6	1:50	4.0 g	3.93 g	98.3 %	Light yellow, compressible
Choline chloride: lactic acid (9:1)	DES-16-MC6	1:50	4.0 g	3.41 g	85.3 %	Light brown, compressible

In general, it appeared that the DES was effective at removing lignin from the TMP. This did not improve the filtration efficiency of the fibers. Pulp was analyzed before and after treatment with DES by SEM. Figure 3-14 shows the SEM images of Line 1 Latency (L1LAT) pulp unmodified, with DES14-A treatment, and DES-14-B treatment. Figure 3-14 (B) demonstrates how DES disrupts the fibers of wood pulp. DES-14-B had the same reaction conditions as DES-14-A, but DES-14-B encountered improper mixing. Figure 3-14 (C) demonstrates the result of this improper mixing as shown by less disruption of the fibers. Interestingly, DES-14-B had a higher filtration efficiency when compared to DES-14-A.

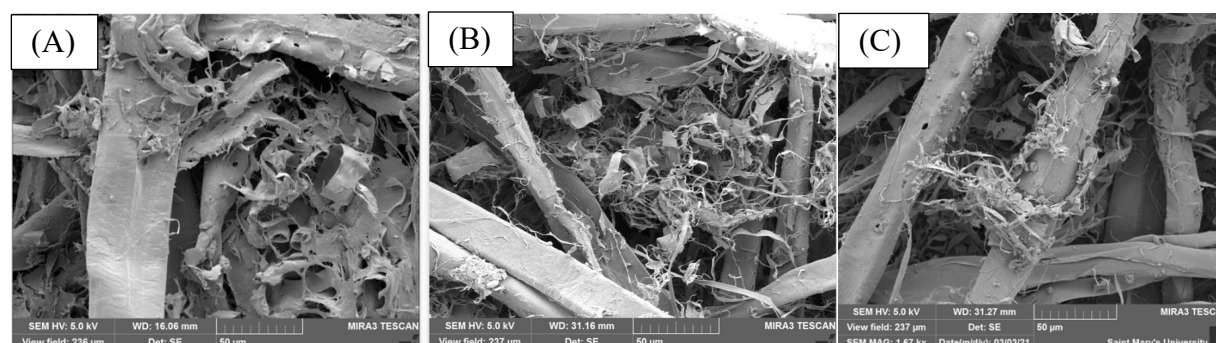


Figure 3-14: L1LAT Pulp (A) Untreated, (B) DES14-A Treated, DES14-B Treated. SEM (voltage: 5.0 keV, Det: SE, Tescan MIRA3 LMU Field Emission SEM).

3.4 Sheet Thickness

The thickness of 20 areas on the paper sheets was measured to determine how uniform the sheet thickness is when prepared manually. Thickness measurements are made using a digital caliper. Initially, the thickness of already approved N95 masks was recorded (Table 3-4). After which, the thickness of the paper sheets were characterized (Table 3-5). Overall, paper sheets produced manually were made within the thickness range of the filter layer on commercial masks.

Table 3-4: The thickness of various combinations of N95 mask layers. Compressed here refers to if pressure is placed on the material during thickness measurements.

Mask Layer(s)	3M N95 Mask	Degil N95 Mask
Uncompressed 3 layers	2.70 mm	1.62 mm
Compressed 3 layers	1.33 mm	0.67 mm
Compressed Filter Layer	0.36 mm	0.22 mm

Table 3-5: The thickness of each of the tested paper sheets.

Sheet Type	Average Thickness (mm)	Standard Deviation (mm)
Unmodified 12g R2B	1.29	0.08
Harmac K10s as Received	1.26	0.05
Unmodified 5g R2B	0.71	0.13
Harmac K10s sheet	0.35	0.04
Unmodified 2g R1B	0.25	0.05
Unmodified 2g R2B	0.25	0.04
R2B DES – 07 – A & B – Oxalic acid – ChCl	0.27	0.02
R2B DES - 09 - Urea-ChCl	0.30	0.04
Line 1 Latency (L1LATTL) Unmodified	0.35	0.03
L1LATTL DES - 10 - Urea - ChCl	0.29	0.06
L1LATTL DES -11- Urea – ChCl	0.27	0.05
L1LATTL DES-12 - Urea - ChCl	0.28	0.06
L1LATTL DES-13 - Urea – ChCl	0.28	0.07
L1LATTL DES-14-A - Urea - ChCl	0.20	0.02
L1LATTL DES-14-B - Urea - ChCl	0.23	0.04
TWP4	0.22	0.02
Sreen Accepts	0.26	0.02
MC6 as Received	0.19	0.06
Scrn. Acpts as Received	0.13	0.01
LATTL2 as Received	0.21	0.02

MC6 - More Clay (MC)	0.32	0.03
MC6 – Less Clay (LC)	0.31	0.03
MC6 – LC – DES-15 – Urea – ChCl – 6 hr 80°C	0.19	0.03
MC6 – LC – DES-16 – Lactic acid – ChCl – 4 hr 80°C	0.34	0.03
Final Product Uncalendared as Received	0.08	0.00
Final Product Super Calendared as Received	0.04	0.00

3.5 Fluorescence Spectroscopy: Filtration Efficiency

The excitation and emission scans of the 0.1 μm fluorescent bead suspension are shown below in Figure 3-15. The fluorophore, a red fluorescent dye, used in these initial studies came from the sulfate-modified polystyrene 100 nm in diameter latex beads. A calibration curve was constructed to determine the linear dynamic range of the Agilent Cary Eclipse fluorescence spectrophotometer for this fluorophore. Initially, the concentrations selected to construct this calibration curve (Figure 3-15) gave a very weak fluorescence intensity. A second calibration curve was constructed with more concentrated standards of the fluorophore to give a greater fluorescence intensity range (Figure 3-16). Any curvature seen in the following fluorescent calibration curves may be attributed to self-absorbance at high concentrations.

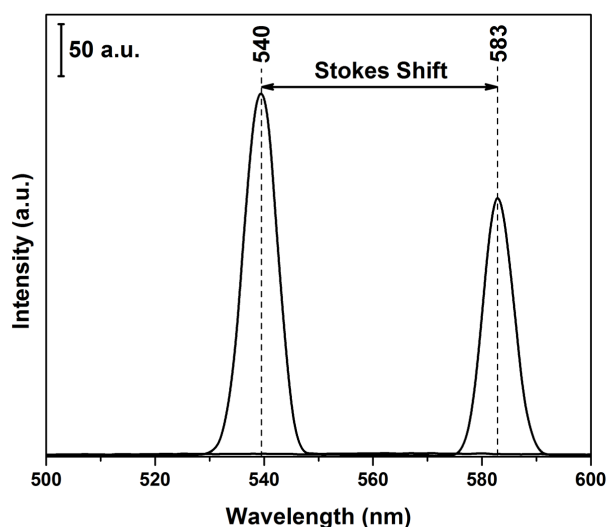


Figure 3-15: The excitation and emission scans stacked for a 1.56×10^{-4} % solids 0.1 μm fluorescent bead suspension. The excitation peak appeared at 540 nm and the emission peak appeared at 583 nm. Fluorescent scans were taken using a Agilent Cary Eclipse fluorescence spectrophotometer.

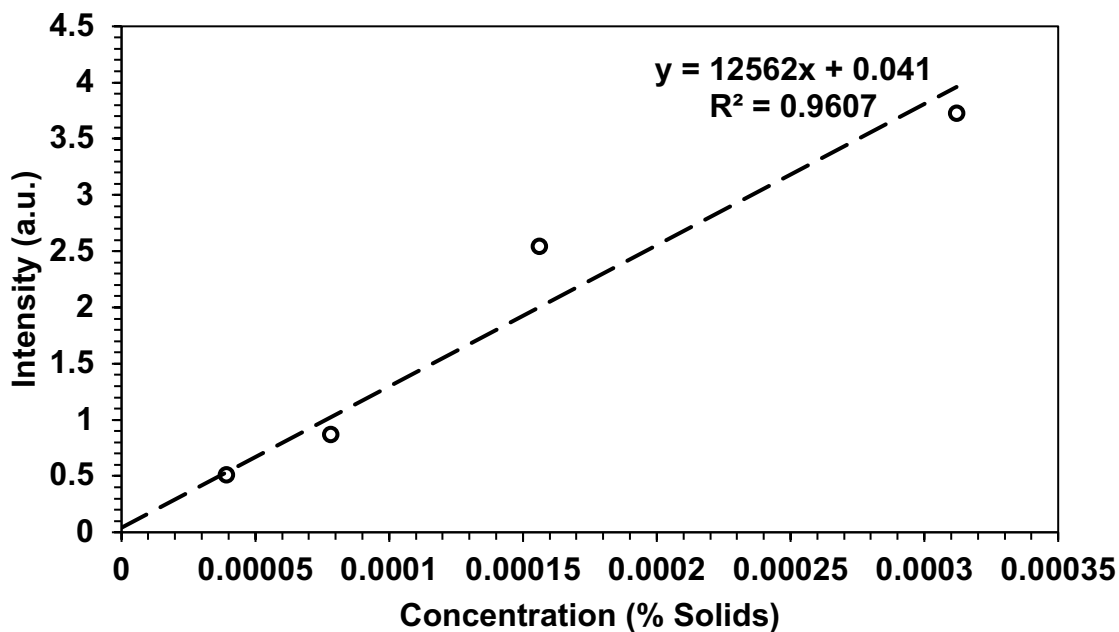


Figure 3-16: The more dilute calibration curve for the 0.1 μm fluorescent bead suspension in ASTM Type 1 water.

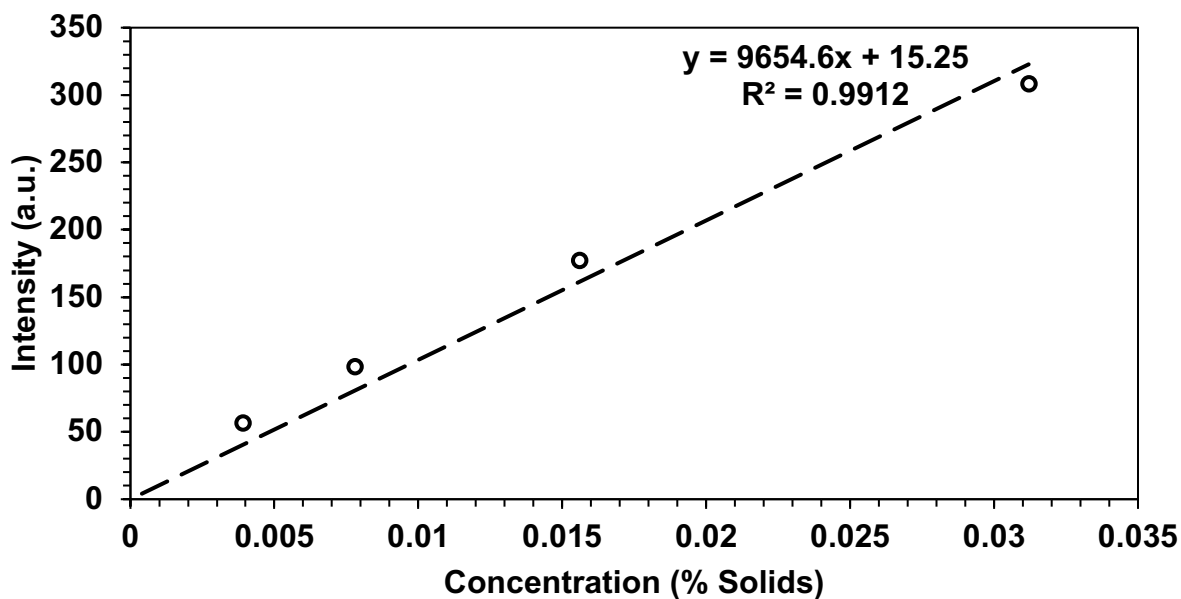


Figure 3-17: The calibration curve for the 0.1 μm fluorescent bead suspension in ASTM Type 1 water.

The signal limit of detection (LOD) of the Agilent Cary Eclipse fluorescence spectrophotometer was calculated (Equation 3-1) using the average of ten blank, ASTM Type 1

water, fluorescence intensity readings (Table 3-7). The LOD was found to be 0.341 a.u. for the 0.1 μm fluorophore.

Table 3-6: The 10 blank reads taken with $\lambda_{\text{ex}} = 540 \text{ nm}$ and $\lambda_{\text{em}} = 583 \text{ nm}$ of ASTM Type 1 water.

Measurement	Intensity (a.u.)
1	0.023
2	-0.075
3	-0.051
4	-0.174
5	0.074
6	0.197
7	-0.050
8	-0.149
9	0.122
10	0.001
Mean	-0.008
SD	0.117

$$\begin{aligned} \text{Limit of Detection (LOD)} &= 3\sigma + \bar{\sigma} \\ \text{LOD} &= ((3) \times (0.117 \text{ a. u.})) + (-0.008 \text{ a.u.}) \\ \text{LOD} &= 0.341 \text{ a. u.} \end{aligned}$$

Equation 3-1: Calculating the Limit of Detection of the Agilent Cary Eclipse fluorescence spectrophotometer.

Initially, the fluorophore was filtered through a Buchner funnel. The results of the Buchner funnel filtration efficiency test with a 0.25 mm thick R1B filter are not shown because there is a theoretical dilution expected in the filtrate due to the presence of water from the required rinsing of the Buchner funnel that creates the seal with the filter paper. The actual measured fluorescence in this study was above that of the theoretical dilution, therefore indicating a negative filtration efficiency, or in other words, the filtrate became concentrated. It was hypothesized that this unexpected result was due to the small size of the fluorophore and its potential to pass through the sides of the filter into the Buchner funnel. To combat this issue future studies used a Micro Filtration System (MFS) designed for filtering of small particles. This 0.1 μm fluorophore was used in a filtration study in the MFS with a 0.25 mm thick R1B filter that was found to have a

filtration efficiency of 0.58 % (Table 3-8). Additionally, a filtration experiment was run with the 0.1 μm fluorophore, in the MFS, with a 0.25 mm thick R2B filter that was found to have a filtration efficiency of 0.87 % (Table 3-8). The filtration efficiency of the k10s pulp was tested in the MFS with the 0.1 μm fluorophore and a 1.25 mm thick k10s filter, which was found to have a filtration efficiency of 6.64 % (Table 3-8). Studies with 100 nm beads gave very low filtration efficiencies. To compare with the k10s filter, a 1.29 mm R2B filter was tested with the 0.1 μm fluorophore, and was found to have a filtration efficiency of -9.04 % (Figure 18). This negative filtration efficiency indicates the filtrate became concentrated, which is proposed to have occurred due to water absorbing on the surface of the thick R2B filter while the fluorescent beads passed through. Negative results are reported as not applicable because they are meaningless values.

Table 3-7: The filtration efficiency of 0.1 μm latex beads by each sheet.

Sample	Filtration Efficiency (%)
R1B - 0.25 mm	0.58
R2B - 0.25 mm	0.87
K10s - 1.26 mm	6.64
R2B - 1.29 mm	N/A

The second fluorophore used was a carboxylate-modified 0.3 μm microparticle. To start, a calibration curve was constructed (Figure 3-18) to determine the linear dynamic range of this fluorophore. A concentration of 0.003 % solids was selected for filtration testing. A 0.30 mm R2B filter was tested in the MFS with the 0.3 μm fluorophore and it was found to have a filtration efficiency of 6.34 %. To validate the reproducibility of this filtration method the filtration efficiency of three different R2B paper sheet samples is reported in Table 3-8. The coefficients of variance describing the thickness and filtration efficiency of these three samples were found to be 6.57 % and 12.63 % respectively. Table 3-9 summarizes the filtration efficiency for each test filter sheet. Two promising candidates include the final product uncalendared and the final product super

calendared. These samples have very few gaps for small particles to pass by and resultantly are giving a higher value for filtration efficiency. SEM images of the final products fiber arrangement are presented below in Figure 3-19. The super calendared final product gave a higher filtration efficiency than the uncalendared product, which is in agreement with the SEM image showing more gaps in the uncalendared surface.

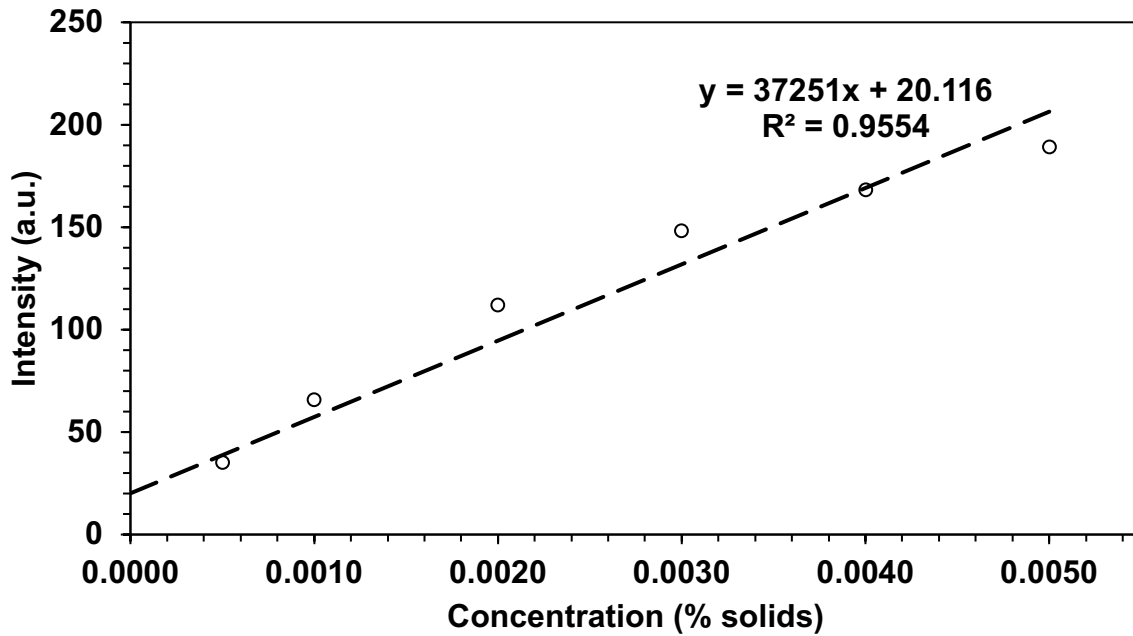


Figure 3-18: The calibration curve for the 0.3 μm fluorescent bead suspension in ASTM Type 1 water.

Table 3-8: Triplicate filtration efficiency study with R2B pulp for method validation.

Sample	Thickness (mm)	Filtration Efficiency (%)
R2B-1	0.31	1.77
R2B-2	0.30	2.01
R2B-3	0.34	2.28

Table 3-9: Summary of 300 nm filtration efficiency results determined using fluorescence spectroscopy.

Sample	Filtration Efficiency (%)
MC6 - 0.19 mm**	17.4
Line 2 Latency - 0.21 mm**	15.5
Screen Accept - 0.13 mm**	11.7
R2B - 0.30 mm	6.34
R2B DES – 07 – A & B – Oxalic acid – ChCl - 0.27 mm	6.40
R2B DES - 08 – Oxalic acid – ChCl – N/A	N/A*
R2B DES - 09 - Urea - ChCl - 0.30 mm	N/A
Line 1 Latency (L1LATTL) - 0.35 mm	7.30
L1LATTL DES - 10 - Urea - ChCl - 0.29 mm	1.50
L1LATTL DES -11- Urea – ChCl – 0.27 mm	2.54
L1LATTL DES-12 - Urea - ChCl - 6hr 100°C – 0.28 mm	2.80
L1LATTL DES-13 - Urea – ChCl - 6hr 80°C – 0.28 mm	3.79
L1LATTL DES-14-A - Urea - ChCl - 1 hr 80°C - 0.20 mm	2.78
L1LATTL DES-14-B - Urea - ChCl - 1 hr 80°C – 0.23 mm	5.92
Screen Accept - 0.26 mm	10.5
TWP – 0.22 mm	2.75
MC6 - More Clay – 0.32 mm	6.24
MC6 – Less Clay – 0.31 mm	11.75
MC6 – Less Clay – DES-15 – Urea – ChCl – 6 hr 80°C – 0.19 mm	3.40
MC6 – Less Clay – DES-16 – Lactic acid – ChCl – 4 hr 80°C – 0.34 mm	1.74
Final Product Uncalendared – 0.08 mm**	7.15
Final Product Super Calendared – 0.04 mm**	10.92

*Fibers were too fine to form a paper sheet. N/A results are under LOD

**Hand sheet formed by Port Hawkesbury using a sheet machine.

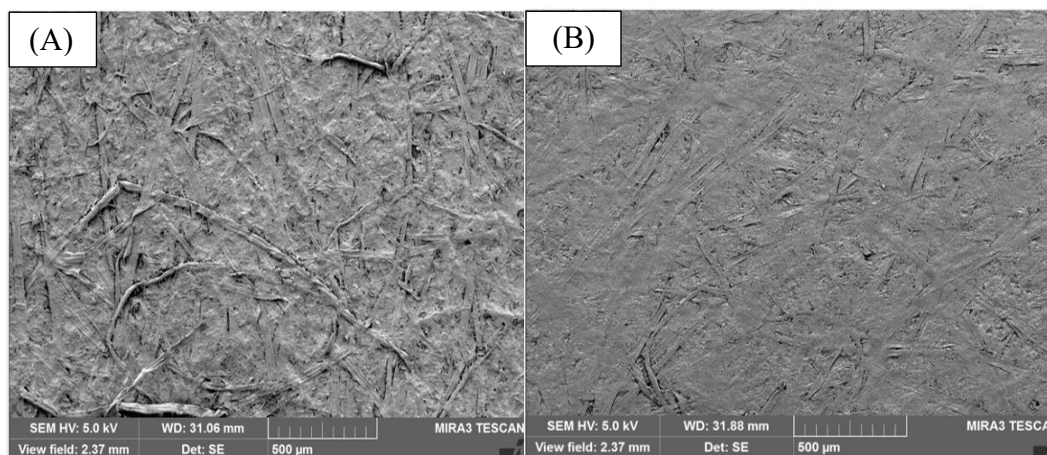


Figure 3-19: The final paper products produced by Port Hawkesbury both (A) Uncalendared and (B) Super-Calendared. SEM (voltage: 5.0 keV, Det: SE, Tescan MIRA3 LMU Field Emission SEM).

Overall, sheets formed at Port Hawkesbury in a sheet machine were found to have a higher filtration efficiency than sheets formed using the paper screen method. The final products provided by Port Hawkesbury show a great deal of promise because of their high filtration capabilities and very small thicknesses. Between the two final products tested the super-calendared sample is performing better. Of the sheets formed using the paper screen method, the MC6 sample with a lower clay content provided the highest filtration efficiency.

3.6 Aerosol Tests

Aerosol testing was conducted using a 3M 6000 series facemask with removable filter attachments. This set up allowed for certified P100 and N95 masks to be tested as controls in addition to experimental conditions where the wood pulp sheet is in the filter holder. Initially, fit factors of zero were recorded on the mannequin head. To solve this problem a molding agent was added to the mannikins face to enhance the fit and reduce any face-seal leakage being recorded by the PortaCount. Results of fit factors measured in these experiments are summarized in Table 3-10.

Table 3-10: Fit Factors obtained from the Porta Count 8038 on a mannequin wearing a 3M 6000 series reusable respirator.

Filter 1	Filter 2	Fit-Factor
P100 3M 2097 NIOSH	P100 3M 2097 NIOSH	1678
MC6 - Less Clay - Thin - Side over hang	P100 3M 2097 NIOSH	33
MC6 Less Clay Thin	P100 3M 2097 NIOSH	13
MC6 Less Clay Thick	P100 3M 2097 NIOSH	6
MC6 More Clay Thick	P100 3M 2097 NIOSH	3
Uncalendered Final Product (1 ply) - Side over hang	P100 3M 2097 NIOSH	79
Uncalendered Final Product (2 ply) - Side over hang	P100 3M 2097 NIOSH	215
Uncalendered Final Product (2 ply) - Side over hang	Uncalendered Final Product (2 ply) - Side over hang	6

7093 3M NIOSH P100 Particulate Filter	7093 3M NIOSH P100 Particulate Filter	2281
Super-calendered Final Product (2 ply) - Side over hang	P100 3M 2097 NIOSH	192
Super-calendered Final Product (1 ply) - Side over hang	P100 3M 2097 NIOSH	341
R2B	P100 3M 2097 NIOSH	82
L1LATT	P100 3M 2097 NIOSH	50
DES 15 – Side over hang	P100 3M 2097 NIOSH	32

A high fit factor indicates low face seal leakage and low filter penetration. Since the mask was not moved off of the mannequin’s head for the duration of these experiments, the face-seal leakage variation between measurements is assumed to be minimal. Therefore, differences in fit factor are attributed to differences in filter penetration. Overall, one P100 filter and one test filter were used for the majority of experiments such that the fit factor would be larger and have less associated error. When the filter overhung the sides of the filter holder it performed better, this is likely because there are less aerosols able to leak inside of the mask. When comparing MC6 samples less clay content and a thinner filter performed better. Calendered and 2 ply was found to perform better than uncalendered and 1 ply. The DES-15 treated MC6 with overhang, and a lower clay content performs almost exactly the same as the untreated MC6 with a low clay content and overhang.

Chapter 4: Conclusions

Overall, this work has shown how PPE is currently produced and has identified goals to aim towards in designing more sustainable PPE options, including: a direct focus on breathability, optimizing fiber width, as well as filtration efficiency and sustainability. Pulp from Port Hawkesbury Paper has been characterized from many different sections along the paper production line including analysis of the paper end product. This Nova Scotian pulp was compared to kraft pulp, cellulose based materials, and synthetically based textiles.

Lignin was identified early on as an important target to remove from the wood pulp in this thesis project. Lignin causes decreased breathability, increased brittleness, and decreased product strength. Lignin content was characterized by kappa number titration, SEM, and IR. Deep eutectic solvents were selected for the removal of lignin from wood pulp because they only require a small amount of energy consumption to be produced, are synthesized in high yields, are environmentally friendly, and result in a thermally stable solvent. DES were successful in the removal of lignin from the wood pulp, yet the filtration efficiency of the material did not increase. This result supports that the presence of lignin may not play as important of a role in filtration efficiency as initially hypothesized. This work on pulp treatment with various DES systems may still be useful for the transformation of biomass into PPE. Since DES are capable of removing lignin, and therefore can increase product strength and breathability, this treatment may prove useful in the creation of more biodegradable PPE besides from masks, such as surgical gowns.

Additionally, this thesis work determined the impact of chemical treatment on small particle filtration. Filtration of nanometer scale fluorescent beads was paired with a Fluorescence

Spectrophotometer to calculate filtration efficiency. One major drawback of this technique is that the use of a wet filtration method negatively influenced the filtration efficiency of the wood pulp based filters. Lastly, this work looks at the ability of wood pulp to filter sodium chloride aerosols in the ambient room concentration in comparison to regulation P100 respirators.

Although a prototype mask was not made, a good initial step was the ability to create wood pulp filters for reusable 3M 6000 series respirators. Although these are not as commonly used by the general population, these reusable respirators present a helpful template for the testing and rapid comparison of new materials. Furthermore, unmodified Port Hawkesbury pulp has shown promise in its similarities to commercially produced PPE. Specifically, their pulp may be applicable in the production of cellulose based fabrics for use in the comfort layers of masks and biodegradable PPE.

Chapter 5: Future Work

Future work on this project should focus on aerosol testing and moving towards more standardized experimental procedures. One limitation of this work was lack of access to standard pulp and paper instrumentation such as a disintegrator and a sheet forming machine. Continuation of this project would be aided by partnerships with industry professionals able to provide access to a sheet former and instrumentation required for proper aerosol testing.

Further physical modification techniques should be explored such as sonification, ball milling, and disintegration. These techniques should be explored to see if they are able to alter pulp fibers advantageously for increased filtration capabilities. Another interesting avenue that was not explored in this work is the impact of freeze drying on the structural arrangement of pulp fibers. Since pulp fibers experience a problem of re-bonding known as hornification, freeze drying is one possible technique that can be used to maintain pulp fibrillation in the dry state. Additionally, the impact of filter paper density should be investigated to determine how decreases in paper density impact filtration efficiency.

The pulp candidates showing the highest filtration efficiency, such as the test sheets received from Port Hawkesbury Paper, warrant further inquiry about how to take part in formal NIOSH approved aerosol testing. Additionally, the paper forming process should be optimized and paper additives should be considered. Lastly, a prototype mask should be produced that is completely biodegradable if a pulp candidate is shown to be capable of a sufficient filtration efficiency.

Chapter 6: References

- (1) Friese, C. R.; Veenema, T. G.; Johnson, J. S.; Jayaraman, S.; Chang, J. C.; Clever, L. H. Respiratory Protection Considerations for Healthcare Workers During the COVID-19 Pandemic. *Health Secur.* **2020**.
- (2) Roser, M.; Ritchie, H.; Ortiz-Ospina, E.; Hasell, J. Coronavirus (COVID-19) Cases <https://ourworldindata.org/covid-cases> (accessed Jun 1, 2020).
- (3) Roser, M.; Ritchie, H.; Ortiz-Ospina, E.; Hasell, J. Coronavirus (COVID-19) Cases <https://ourworldindata.org/covid-cases> (accessed Nov 27, 2020).
- (4) Blachere, F. M.; Lindsley, W. G.; McMillen, C. M.; Beezhold, D. H.; Fisher, E. M.; Shaffer, R. E.; Noti, J. D. Assessment of Influenza Virus Exposure and Recovery from Contaminated Surgical Masks and N95 Respirators. *J. Virol. Methods* **2018**, *260*, 98–106.
- (5) Roser, M.; Ritchie, H.; Ortiz-Ospina, E.; Hasell, J. Canada: Coronavirus Pandemic Country Profile <https://ourworldindata.org/coronavirus>.
- (6) Guan, W.; Ni, Z.; Hu, Y.; Liang, W.; Ou, C.; He, J.; Liu, L.; Shan, H.; Lei, C.; Hui, D. S. Clinical Characteristics of Coronavirus Disease 2019 in China. *N Engl J Med* **2020**, *382*, 1708–1720.
- (7) National Institute for Occupational health and safety (NIOSH). *42 CFR, Part 84, Respiratory Protective Devices: Final Rules and Notice*; 1997.
- (8) Qian, Y.; Willeke, K.; Grinshpun, S. A.; Donnelly, J.; Coffey, C. C. Performance of N95 Respirators: Filtration Efficiency for Airborne Microbial and Inert Particles. *Am. Ind. Hyg. Assoc. J.* **1998**, *59* (2), 128–132.
- (9) Mao, J.; Grgic, B.; Finlay, W. H.; Kadla, J. F.; Kerekes, R. J. Wood Pulp Based Filters for Removal of Sub-Micrometer Aerosol Particles. *Nord. Pulp Pap. Res. J.* **2008**, *23* (4), 420–425.
- (10) Rengasamy, A.; Zhuang, Z.; BerryAnn, R. Respiratory Protection against Bioaerosols: Literature Review and Research Needs. *Am. J. Infect. Control* **2004**, *32* (6), 345–354.
- (11) Zhou, S. S.; Lukula, S.; Chiossone, C.; Nims, R. W.; Suchmann, D. B.; Ijaz, M. K. Assessment of a Respiratory Face Mask for Capturing Air Pollutants and Pathogens Including Human Influenza and Rhinoviruses. *J. Thorac. Dis.* **2018**, *10* (3), 2059.
- (12) Staymates, M. Flow Visualization of an N95 Respirator with and without an Exhalation Valve Using Schlieren Imaging and Light Scattering. *Phys. Fluids* **2020**, *32* (11), 111703. <https://doi.org/10.1063/5.0031996>.
- (13) Osong, S.; Norgren, S.; Engstrand, P. Processing of Wood-Based Microfibrillated Cellulose and Nanofibrillated Cellulose, and Applications Relating to Papermaking: A Review. *Cellulose* **2016**, *23* (1), 93–123. <https://doi.org/10.1007/s10570-015-0798-5>.
- (14) Xu, W.; Wang, X.; Sandler, N.; Willför, S.; Xu, C. Three-Dimensional Printing of Wood-Derived Biopolymers: A Review Focused on Biomedical Applications. *ACS Sustain. Chem. Eng.* **2018**, *6* (5), 5663–5680.
- (15) Samyn, P.; Barhoum, A.; Öhlund, T.; Dufresne, A. Nanoparticles and Nanostructured Materials in Papermaking. *J. Mater. Sci.* **2018**, *53* (1), 146–184.
- (16) Whetten, R.; Sederoff, R. Lignin Biosynthesis. *Plant Cell* **1995**, *7* (7), 1001–1013. <https://doi.org/10.1105/tpc.7.7.1001>.
- (17) Zhu, H.; Jia, Z.; Chen, Y.; Weadock, N.; Wan, J.; Vaaland, O.; Han, X.; Li, T.; Hu, L. Tin Anode for Sodium-Ion Batteries Using Natural Wood Fiber as a Mechanical Buffer and Electrolyte Reservoir. *Nano Lett.* **2013**, *13* (7), 3093. <https://doi.org/10.1021/nl400998t>.

- (18) Metreveli, G.; Wågberg, L.; Emmoth, E.; Belák, S.; Strømme, M.; Mihranyan, A. A Size-Exclusion Nanocellulose Filter Paper for Virus Removal. *Adv. Healthc. Mater.* **2014**, *10* (3), 1546–1550.
- (19) Bleumink, E.; Mitchell, J.; Nater, J. Allergic Contact Dermatitis from Cedar Wood (*Thuja Plicata*). *Br. J. Dermatol.* **1973**, *88* (5), 499–504.
- (20) Subramanian, R.; Kononov, A.; Kang, T.; Paltakari, J.; Paulapuro, H. Structure and Properties of Some Natural Cellulosic Fibrils. *BioResources* **2008**, *3* (1), 192–203.
- (21) Hult, E.-L.; Koivu, K.; Asikkala, J.; Ropponen, J.; Wrigstedt, P.; Sipilä, J.; Poppius-Levlin, K. Esterified Lignin Coating as Water Vapor and Oxygen Barrier for Fiber-Based Packaging. *Holzforschung* **2013**, *67* (8), 899–905. <https://doi.org/10.1515/hf-2012-0214>.
- (22) Kapoor, A.; Baronia, A. K.; Azim, A.; Agarwal, G.; Prasad, N.; Mishra, R.; Saraswat, V. A. Breathability and Safety Testing of Personal Protective Equipment: “Human-Comfort” Factor Remains Undefined. *Indian J. Crit. Care Med. Peer-Rev. Off. Publ. Indian Soc. Crit. Care Med.* **2021**, *25* (1), 12–15. <https://doi.org/10.5005/jp-journals-10071-23598>.
- (23) Laurichesse, S.; Avérous, L. Chemical Modification of Lignin: Towards Bio Based Polymers. *Prog. Polym. Sci.* **2014**, *39* (7), 1266–1290.
- (24) Duval, A.; Lawoko, M. A Review on Lignin-Based Polymeric, Micro- and Nano-Structured Materials. *React. Funct. Polym.* **2014**, *85*, 78–96.
- (25) Li, K.; Lei, X.; Lu, L.; Camm, C. Surface Characterization and Surface Modification of Mechanical Pulp Fibres. *Pulp Pap. Can.* **2010**, *111* (1), 28–33.
- (26) Shao, Z.; Li, K. The Effect of Fiber Surface Lignin on Interfiber Bonding. *J. Wood Chem. Technol.* **2006**, *26* (3), 231–244. <https://doi.org/10.1080/02773810601023438>.
- (27) Douek, M. Pulp and Paper Matrices. In *Encyclopedia of Analytical Chemistry*; American Cancer Society, 2006; pp 1–26. <https://doi.org/10.1002/9780470027318.a2209>.
- (28) Alves, A.; Schwanninger, M.; Pereira, H.; Rodrigues, J. Calibration of NIR to Assess Lignin Composition (H/G Ratio) in Maritime Pine Wood Using Analytical Pyrolysis as the Reference Method. **2006**, *60* (1), 29–31. <https://doi.org/10.1515/HF.2006.006>.
- (29) Lupoi, J. S.; Singh, S.; Simmons, B. A.; Henry, R. J. Assessment of Lignocellulosic Biomass Using Analytical Spectroscopy: An Evolution to High-Throughput Techniques. *BioEnergy Res.* **2014**, *7* (1), 1–23. <https://doi.org/10.1007/s12155-013-9352-1>.
- (30) Jiang, J.; Carrillo-Enriquez, N. C.; Oguzlu, H.; Han, X.; Bi, R.; Song, M.; Saddler, J. N.; Sun, R.-C.; Jiang, F. High Production Yield and More Thermally Stable Lignin-Containing Cellulose Nanocrystals Isolated Using a Ternary Acidic Deep Eutectic Solvent. *ACS Sustain. Chem. Eng.* **2020**, *8* (18), 7182–7191. <https://doi.org/10.1021/acssuschemeng.0c01724>.
- (31) Clarke, C. J.; Tu, W.-C.; Levers, O.; Bröhl, A.; Hallett, J. P. Green and Sustainable Solvents in Chemical Processes. *Chem. Rev.* **2018**, *118* (2), 747–800. <https://doi.org/10.1021/acs.chemrev.7b00571>.
- (32) Ashworth, C. R.; Matthews, R. P.; Welton, T.; Hunt, P. A. Doubly Ionic Hydrogen Bond Interactions within the Choline Chloride–Urea Deep Eutectic Solvent. *Phys. Chem. Chem. Phys.* **2016**, *18* (27), 18145–18160.
- (33) Wang, S.; Li, H.; Xiao, L. P.; Song, G. Unraveling the Structural Transformation of Wood Lignin During Deep Eutectic Solvent Treatment. *Front. Energy Res* **2020**, *8*, 48.
- (34) Tang, B.; Row, K. H. Recent Developments in Deep Eutectic Solvents in Chemical Sciences. *Monatshfte Für Chem. - Chem. Mon.* **2013**, *144* (10), 1427–1454. <https://doi.org/10.1007/s00706-013-1050-3>.

- (35) Yu, W.; Wang, C.; Yi, Y.; Wang, H.; Zeng, L.; Li, M.; Yang, Y.; Tan, Z. Comparison of Deep Eutectic Solvents on Pretreatment of Raw Ramie Fibers for Cellulose Nanofibril Production. *ACS Omega* **2020**, *5* (10), 5580–5588. <https://doi.org/10.1021/acsomega.0c00506>.
- (36) Schilling, K.; Gentner, D.; Wilen, L.; Medina, A.; Buehler, C.; Perez-Lorenzo, L. J.; Pollitt, K. J. G.; Bergemann, R.; Bernardo, N.; Peccia, J. An Accessible Method for Screening Aerosol Filtration Identifies Poor-Performing Commercial Masks and Respirators. **2020**.
- (37) Faridi, S.; Nodehi, R. N.; Sadeghian, S.; Tajdini, M.; Hoseini, M.; Yunesian, M.; Nazmara, S.; Hassanvand, M. S.; Naddafi, K. Can Respirator Face Masks in a Developing Country Reduce Exposure to Ambient Particulate Matter? *J. Expo. Sci. Environ. Epidemiol.* **2020**, *30* (4), 606–617.
- (38) Froass, P. M.; Ragauskas, A. J.; Jiang, J. Nuclear Magnetic Resonance Studies. 4. Analysis of Residual Lignin after Kraft Pulping. *Ind. Eng. Chem. Res.* **1998**, *37* (8), 3388–3394. <https://doi.org/10.1021/ie970812c>.
- (39) Iiyama, K.; Wallis, A. F. A. An Improved Acetyl Bromide Procedure for Determining Lignin in Woods and Wood Pulps. *Wood Sci. Technol.* **1988**, *22* (3), 271–280. <https://doi.org/10.1007/BF00386022>.
- (40) Lee, R. A.; Bédard, C.; Berberi, V.; Beauchet, R.; Lavoie, J.-M. UV–Vis as Quantification Tool for Solubilized Lignin Following a Single-Shot Steam Process. *Bioresour. Technol.* **2013**, *144*, 658–663. <https://doi.org/10.1016/j.biortech.2013.06.045>.
- (41) Smink, D.; Juan, A.; Schuur, B.; Kersten, S. R. Understanding the Role of Choline Chloride in Deep Eutectic Solvents Used for Biomass Delignification. *Ind. Eng. Chem. Res.* **2019**, *58* (36), 16348–16357.
- (42) Jiebing, L.; Göran, G. Kinetics and Mechanism of Kappa Number Determination. *Nord. Pulp Pap. Res. J.* **1998**, *13* (2), 147–152. <https://doi.org/doi:10.3183/npprj-1998-13-02-p147-152>.
- (43) Skoog, D.; West, D.; Holler, F.; Crouch, S. *Fundamentals of Analytical Chemistry*, 8th ed.; Nelson Education, 2013.
- (44) Coffey, C. C.; Campbell, D. L.; Myers, W. R. Comparison of Six Respirator Fit-Test Methods with an Actual Measurement of Exposure in a Simulated Health Care Environment: Part III—Validation. *Am. Ind. Hyg. Assoc. J.* **1999**, *60* (3), 363–366.
- (45) Rengasamy, S.; Eimer, B. C.; Shaffer, R. E. Evaluation of the Performance of the N95-Companion: Effects of Filter Penetration and Comparison with Other Aerosol Instruments. *J. Occup. Environ. Hyg.* **2012**, *9* (7), 417–426.
- (46) Duling, M. G.; Lawrence, R. B.; Slaven, J. E.; Coffey, C. C. Simulated Workplace Protection Factors for Half-Facepiece Respiratory Protective Devices. *J. Occup. Environ. Hyg.* **2007**, *4* (6), 420–431. <https://doi.org/10.1080/15459620701346925>.
- (47) TAPPI Standard. *T 236, OM 13. Kappa Number of Pulp*; 2013.
- (48) Jung, S.; Lee, S.; Dou, X.; Kwon, E. E. Valorization of Disposable COVID-19 Mask through the Thermo-Chemical Process. *Chem. Eng. J.* **2021**, *405*, 126658. <https://doi.org/10.1016/j.cej.2020.126658>.
- (49) Varnell, D. F.; Coleman, M. M. FT i.r. Studies of Polymer Blends: V. Further Observations on Polyester-Poly(Vinyl Chloride) Blends. *Polymer* **1981**, *22* (10), 1324–1328. [https://doi.org/10.1016/0032-3861\(81\)90230-5](https://doi.org/10.1016/0032-3861(81)90230-5).
- (50) Najjian, F.; Rudi, H.; Resalati, H.; Torshizi, H. J. Application of Bio-Based Modified Kaolin Clay Engineered as Papermaking Additive for Improving the Properties of Filled

Recycled Papers. *Appl. Clay Sci.* **2019**, *182*, 105258.
<https://doi.org/10.1016/j.clay.2019.105258>.

Chapter 7: Appendix

7.1 SEM Images of Filter Paper Following Filtration

Following filtration all filter papers were imaged using SEM. Figure 7-1 shows the 100 nm fluorescent beads trapped within the fibers of the filter paper test sheets. These images support that the filter paper is retaining some proportion of the beads being passed through during filtration. Figure 7-2 shows the 300 nm fluorescent beads also trapped within the fibers of the filter paper test sheets.

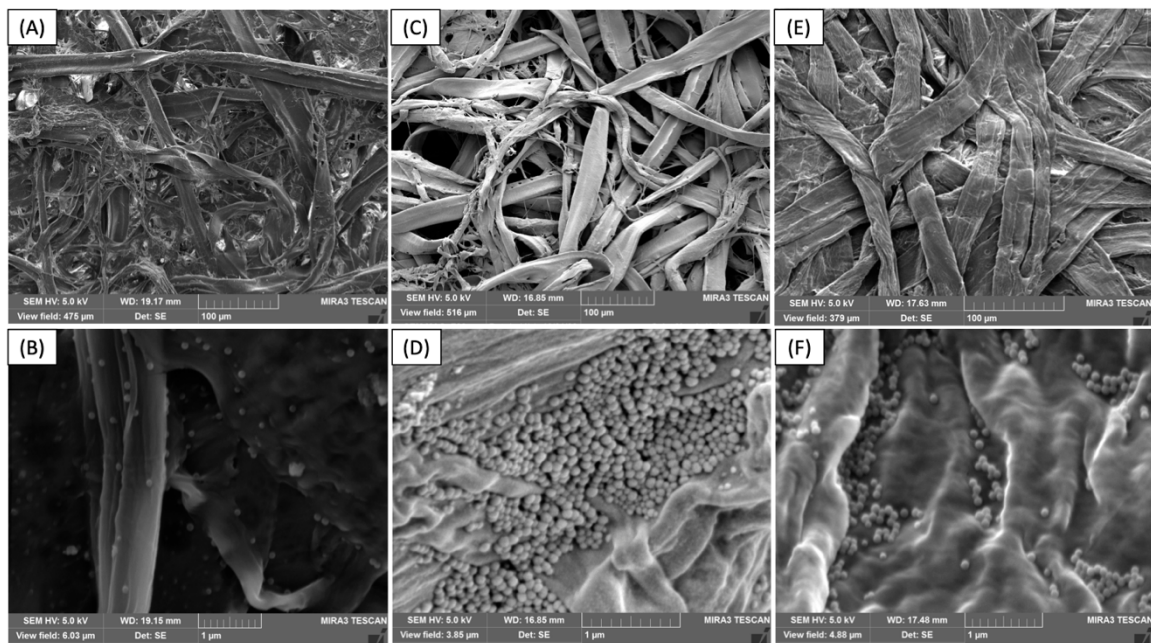


Figure 7-1: The SEM images of filtration paper following filtration of 100 nm fluorescent beads. (A) and (B) are R1B 0.25mm, (C) and (D) are R2B 0.25 mm, (E) and (F) are K10s 1.26 mm. SEM (voltage: 5.0 keV, Det: SE, Tescan MIRA3 LMU Field Emission SEM).

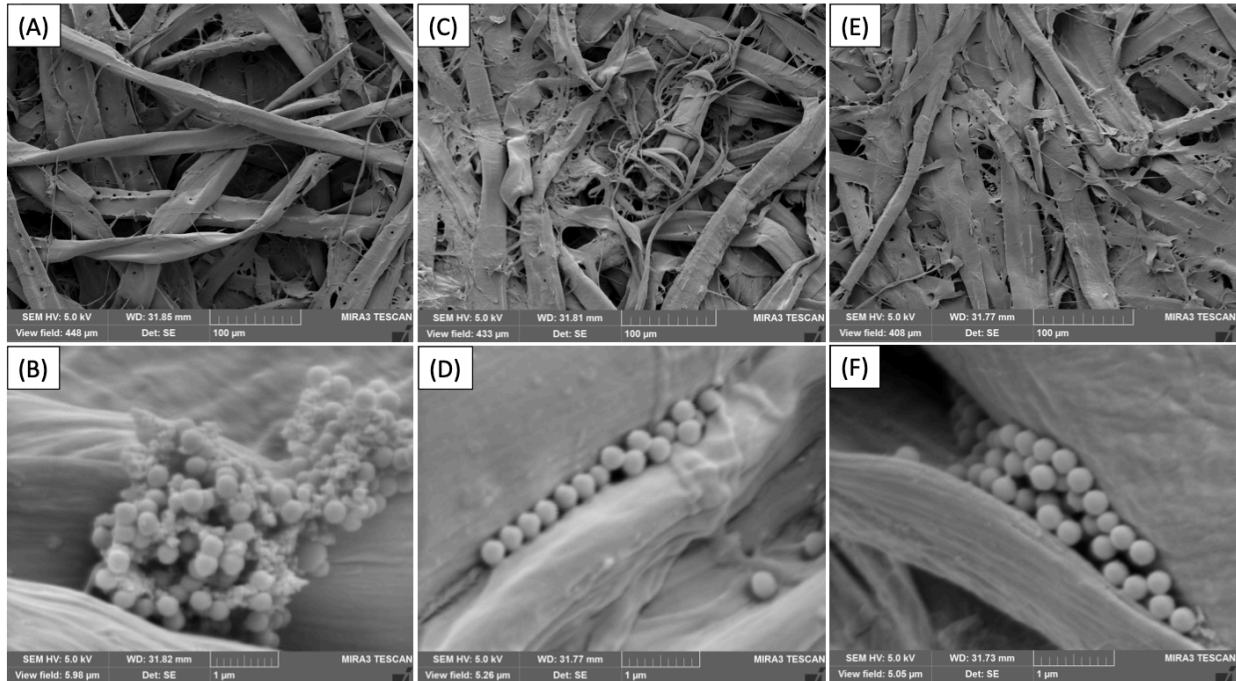


Figure 7-2: The SEM images of filtration paper following filtration of 300 nm fluorescent beads. (A) and (B) are L2LAT, (C) and (D) are R2B, (E) and (F) are Screen Accepts. SEM (voltage: 5.0 keV, Det: SE, Tescan MIRA3 LMU Field Emission SEM).

7.2 Reproduced Figures Letters of Permission

Figure 1-1 is reproduced with permission from Max Roser, Hannah Ritchie, Esteban Ortiz-Ospina and Joe Hasell (2020) - "Coronavirus Pandemic (COVID-19)". *Published online at OurWorldInData.org*. Retrieved from: '<https://ourworldindata.org/coronavirus>' [Online Resource]

Below is a screenshot from the Our World in Data online resource stating permission of reuse.

All the material produced by Our World in Data, including text, interactive visualizations, and code, are completely open access under the [Creative Commons BY license](#). You have the permission to use, distribute, and reproduce these in any medium, provided the source and authors are credited.


Figure 1-3 is reproduced with permission from Qian, Y.; Willeke, K.; Grinshpun, S. A.; Donnelly, J.; Coffey, C. C. Performance of N95 Respirators: Filtration Efficiency for Airborne Microbial and

Inert Particles. *Am. Ind. Hyg. Assoc. J.* **1998**, *59* (2), 128–132. Below is a screenshot from the RightsLink online resource stating permission of reuse.



The screenshot displays the RightsLink interface. At the top left is the Copyright Clearance Center logo. The main header features the RightsLink logo. On the right, there are navigation links: Home, Help, Email Support, and a user profile for Kaleigh McLeod. The main content area shows a Taylor & Francis logo and the title "Performance of N95 Respirators: Filtration Efficiency for Airborne Microbial and Inert Particles". Below the title, it lists the author (Ying-Qian, Klaus Willeke, et al), the publication (Journal of Occupational and Environmental Hygiene), the publisher (Taylor & Francis), and the date (Feb 1, 1998). A note states "Rights managed by Taylor & Francis". Below this, a "Thesis/Dissertation Reuse Request" section is visible, containing the text: "Taylor & Francis is pleased to offer reuses of its content for a thesis or dissertation free of charge contingent on resubmission of permission request if work is published." At the bottom of this section are "BACK" and "CLOSE" buttons.

Figure 1-5 is reproduced with permission from Zhu, H.; Jia, Z.; Chen, Y.; Weadock, N.; Wan, J.; Vaaland, O.; Han, X.; Li, T.; Hu, L. Tin Anode for Sodium-Ion Batteries Using Natural Wood Fiber as a Mechanical Buffer and Electrolyte Reservoir. *Nano Lett.* **2013**, *13* (7), 3093. <https://doi.org/10.1021/nl400998t>. Below is a screenshot from the RightsLink online resource stating permission of reuse.



Tin Anode for Sodium-Ion Batteries Using Natural Wood Fiber as a Mechanical Buffer and Electrolyte Reservoir
Author: Hongli Zhu, Zheng Jia, Yuchen Chen, et al
Publication: Nano Letters
Publisher: American Chemical Society
Date: Jul 1, 2013
Copyright © 2013, American Chemical Society

PERMISSION/LICENSE IS GRANTED FOR YOUR ORDER AT NO CHARGE

This type of permission/license, instead of the standard Terms & Conditions, is sent to you because no fee is being charged for your order. Please note the following:

- Permission is granted for your request in both print and electronic formats, and translations.
- If figures and/or tables were requested, they may be adapted or used in part.
- Please print this page for your records and send a copy of it to your publisher/graduate school.
- Appropriate credit for the requested material should be given as follows: "Reprinted (adapted) with permission from (COMPLETE REFERENCE CITATION). Copyright (YEAR) American Chemical Society." Insert appropriate information in place of the capitalized words.
- One-time permission is granted only for the use specified in your request. No additional uses are granted (such as derivative works or other editions). For any other uses, please submit a new request.

If credit is given to another source for the material you requested, permission must be obtained from that source.

[BACK](#) [CLOSE WINDOW](#)

Figure 1-7 is reproduced with permission from Laurichesse, S.; Avérous, L. Chemical Modification of Lignin: Towards Bio Based Polymers. *Prog. Polym. Sci.* **2014**, *39* (7), 1266–1290.

Below is a screenshot from the RightsLink online resource stating permission of reuse.

This Agreement between Saint Mary's University -- Kaleigh McLeod ("You") and Elsevier ("Elsevier") consists of your license details and the terms and conditions provided by Elsevier and Copyright Clearance Center.

License Number	5043940222530
License date	Apr 07, 2021
Licensed Content Publisher	Elsevier
Licensed Content Publication	Progress in Polymer Science
Licensed Content Title	Chemical modification of lignins: Towards biobased polymers
Licensed Content Author	Stéphanie Laurichesse, Luc Avérous
Licensed Content Date	Jul 1, 2014

Figure 1-10 is reproduced with permission from Metreveli, G.; Wågberg, L.; Emmoth, E.; Belák, S.; Strømme, M.; Mihranyan, A. A Size-Exclusion Nanocellulose Filter Paper for Virus

Removal. *Adv. Healthc. Mater.* **2014**, *10* (3), 1546–1550. Below is a screenshot from the RightsLink online resource stating permission of reuse.

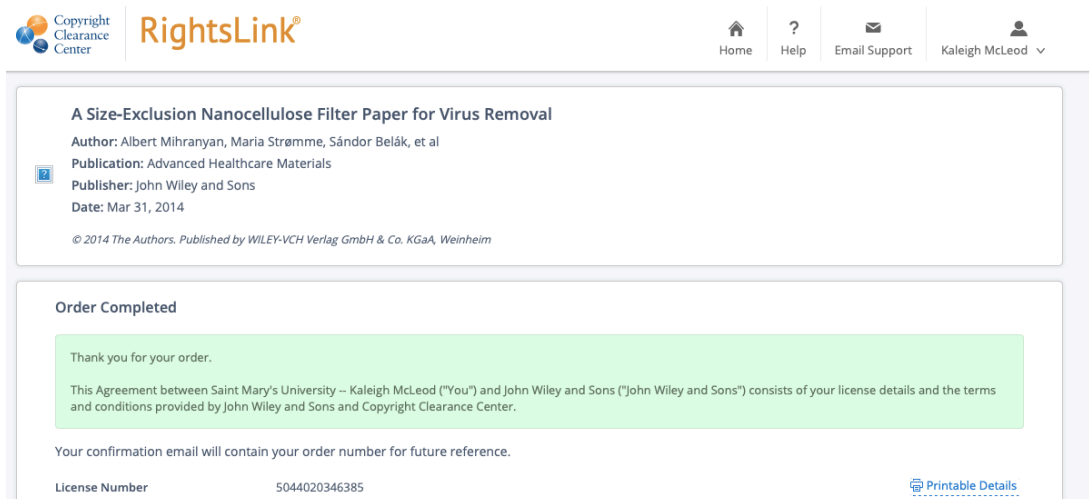


Figure 1-11 is reproduced with permission from Schilling, K.; Gentner, D.; Wilen, L.; Medina, A.; Buehler, C.; Perez-Lorenzo, L. J.; Pollitt, K. J. G.; Bergemann, R.; Bernardo, N.; Peccia, J. An Accessible Method for Screening Aerosol Filtration Identifies Poor-Performing Commercial Masks and Respirators. **2020**. Below is a screenshot from the RightsLink online resource stating permission of reuse.

This Agreement between Saint Mary's University -- Kaleigh McLeod ("You") and Springer Nature ("Springer Nature") consists of your license details and the terms and conditions provided by Springer Nature and Copyright Clearance Center.

License Number	5037981247084
License date	Mar 28, 2021
Licensed Content Publisher	Springer Nature
Licensed Content Publication	Journal of Exposure Science and Environmental Epidemiology
Licensed Content Title	An accessible method for screening aerosol filtration identifies poor-performing commercial masks and respirators
Licensed Content Author	Katherine Schilling et al
Licensed Content Date	Aug 6, 2020
Type of Use	Thesis/Dissertation
Requestor type	academic/university or research institute
Format	print and electronic
Portion	figures/tables/illustrations
Number of figures/tables/illustrations	1
Will you be translating?	no

Figure 1-12 is reproduced with permission from Faridi, S.; Nodehi, R. N.; Sadeghian, S.; Tajdini, M.; Hoseini, M.; Yunesian, M.; Nazmara, S.; Hassanvand, M. S.; Naddafi, K. Can Respirator Face Masks in a Developing Country Reduce Exposure to Ambient Particulate Matter? *J. Expo.*

Sci. Environ. Epidemiol. **2020**, *30* (4), 606–617. Below is a screenshot from the RightsLink online resource stating permission of reuse.

The screenshot displays the RightsLink interface. At the top left is the Copyright Clearance Center logo and the RightsLink® logo. The top right navigation bar includes links for Home, Help, Email Support, and a user profile for Kaleigh McLeod. The main content area is divided into two sections. The first section, titled "Can respirator face masks in a developing country reduce exposure to ambient particulate matter?", lists the author as Sasan Faridi et al, the publication as the Journal of Exposure Science and Environmental Epidemiology, the publisher as Springer Nature, and the date as Apr 21, 2020. It also includes a copyright notice: "Copyright © 2020, The Author(s), under exclusive licence to Springer Nature America, Inc." The second section, titled "Order Completed", contains a green message box that says "Thank you for your order." and "This Agreement between Saint Mary's University – Kaleigh McLeod ('You') and Springer Nature ('Springer Nature') consists of your license details and the terms and conditions provided by Springer Nature and Copyright Clearance Center." Below this, it states "Your confirmation email will contain your order number for future reference." and provides a table with license details.

License Number	5044021266111	Printable Details
License date	Apr 08, 2021	